Response to Reviewer 2's comments

Re: Manuscript essd-2020-16

Earth System Science Data

2020-06-24

Dear Reviewer,

Thank you very much for your time and efforts in reviewing our manuscript and providing encouraging and constructive comments. We have carefully revised the manuscript following your comments/suggestions. The comments are in *italic* and each comment is followed by a response and a description of the tracked change in the manuscript.

With best regards,

Sincerely,

Lei Wang, Dr., Prof.

Key Lab. of Tibetan Environmental Changes and Land Surface Processes,

Institute of Tibetan Plateau Research, Chinese Academy of Sciences

No. 16 Lincui Road, Chaoyang District, Beijing 100101, China

Tel: +86-10-84097107   Fax: +86-10-84097079

Email: wanglei@itpcas.ac.cn

General comment:

Comment 1: *In the paper, the authors integrated five satellite/reanalysis data to generate a new precipitation dataset set in the Yarlung Tsangpo basin in South Tibetan Plateau (TP). Actually, the issue is important for the hydrological studies in TP including this study area, but it is also a difficult issue, as there lacks enough observed data. The authors did a good try to generate this precipitation dataset, and it would be useful for the relevant studies in the basin. Overall, I suggest the authors consider more the following issues before its acceptance.*

Response: Many thanks for your constructive comments. We have revised the manuscript accordingly following your kind suggestions.

Detailed Comments:

Comment 1: *The authors assumed that daily precipitation conforms to a normal distribution. However, precipitation data generally follow skew distribution. The reasonability of this assumption should be discussed more.*

Response: Of course, the assumption of a normal distribution may lead to uncertainty when analyzing extremely high daily precipitation. Generally, the non-normal (skewed) distribution of precipitation is caused by the zero rainfall events at single observational site (Kumar et al., 2009; Semenov, 2008; Sloughter et al., 2007). We calculated the average values of the observed precipitation from 166 rain gauges to reduce the zero rainfall values. Another associated problem is the quantity and reliability of the data that are used to fit the distribution. If we use different probability distributions to describe the observed time series of daily precipitation, different extreme values may be obtained (Angelidis et al., 2012). This study provides a foundation from which further studies can be carried out to explore these aspects in more detail.

Change: We have added discussions and references in the revised manuscript (L360-L366).

Angelidis, P., Maris, F., Kotsovinos, N., and Hrissanthou, V.: Computation of Drought Index SPI with Alternative Distribution Functions. Water Resour. Manage., 26(9), 2453-2473, 2012.

Kumar, M.N., Murthy, C.S., Sai, M.V., and Roy, P.S.: On the use of Standardized Precipitation Index (SPI) for drought intensity assessment. Meteorol. Appl., 16(3), 381-389, 2009.

Semenov, M.A.: Simulation of extreme weather events by a stochastic weather generator. Clim. Res., 35(3), 203-212, 2008.

Sloughter, J.M., Raftery, A.E., Gneiting, T., and Fraley, C.: Probabilistic Quantitative Precipitation Forecasting Using Bayesian Model Averaging. Mon. Weather Rev., 135(9), 3209-3220, 2007.

Comment 2: *Some contents can be added to discuss more about the altitude effects on the quality of the new precipitation data, especially on the IDW practices, although some discussions have been given in Conclusions.*

Response: Thank you for the comments. Generally, these rain gauges were installed at relatively plain area, which may lead to large uncertainty in estimating precipitation (rain or snow) at high mountains, especially in the daily or finer time scales (Ahrens, 2006; Haiden and Pistotnik, 2009). This limitation can be even more severe, due to the orographic effect on precipitation rates, in mountainous regions and transition zones between the low and high altitudes, which will results in the underestimates of the actual basin-wide precipitation (Anders et al., 2006; Hashemi et al., 2020).

Regarding the IDW practices, on the one hand, most of the studied operational precipitation products have already dealt with the altitude effects during data production, and thereby we didn't repeatedly consider the altitude effects when interpolating and integrating these products into 5 km grids with the IDW method. On the other hand, the available gauges (number and distribution) are still far from enough to derive a reasonable spatial distribution of basin-wide altitude gradient for precipitation, due to the complex topography in the study area.

Change: We have added discussions and references in the revised manuscript (L347-L356).

Ahrens, B.: Distance in spatial interpolation of daily rain gauge data. Hydrol. Earth Syst. Sci., 10, 197-208, 2006.

Anders, A.M., Roe, G.H., Hallet, B., Montgomery, D.R., and Putkonen, J.: Spatial patterns of precipitation and topography in the himalaya. Geol. Soc. Am. Spec. Pap., 398, 39-53, 2006.

Haiden, T., and Pistotnik, G.: Intensity-dependent parameterization of elevation effects in precipitation analysis. Adv. Geosci., 33-38, 2009.

Hashemi, H., Fayne, J.V., Lakshmi, V., and Huffman, G.J.: Very high resolution,

altitude-corrected, TMPA-based monthly satellite precipitation product over the CONUS. Sci. Data, 7(1), 2020.

Comment 3: *In lines 252-253, it is interesting to find that the weights become smaller with time periods, why? Is it due more reliable quality of the five datasets in recently years? or due to more observed data used? Some contents can be added to simply explain this.*

Response: We finally adopted the same weight of each product through the trial-and-error method. Table 1 lists the time ranges of different precipitation products, which are very different and lead to different weights during different periods. As a result, during 1981-1997 (only GLDAS, ITP-Forcing, MERRA2 are available), the weight of each product is 1/3. Similarly, during 1998-2007 and 2008-2016, the weights of each product are 1/4 and 1/5 respectively.

Table 1. The precipitation products used in this study.

Precipitation products	Time range	Temporal resolution	Spatial resolution
CMA gridded data	2008-2016	hourly	0.1°×0.1°
GLDAS	1981-2016	3-hour	0.25°×0.25°
ITP-Forcing	1981-2016	3-hour	0.1°×0.1°
MERRA2	1981-2016	hourly	0.5°×0.625°
TRMM	1998-2016	3-hour	0.25°×0.25°

Change: We add some descriptions to explain the weight (L252-L257) in the revised manuscript.

Comment 4: *In Figure 6, does the P_int have similar PDF as the CMA? Why?*

Response: Yes, the PDF of the *P_int* is the closest to that of CMA. Parameters of the normal distribution for the *P_int* and the CMA data are also very similar, with a mean value of 77.0 and 75.3 mm, a standard deviation of 62.3 and 62.6 mm, respectively.

The advantage of the CMA product is that it has incorporated more gauge observations (including many unpublished ones of CMA). The short time duration may be the demerit of this product, since it is only available from 2008.

For our newly integrated data, we have incorporated valuable observational gauge

data from Ministry of Water Resources (MWR), China. This greatly helps us to calibrate and validate the *P_int*.

Therefore, both of two data products have utilized lots of observational information (that provides the ground truth), which leads to the similar PDF.

Change: There is no relevant change in the manuscript.

Comment 5: *This study area should be called "Yarlung Tsangpo" or "Yarlung Zangbo"? please check it.*

Response: This area can be called as "Yarlung Zangbo" or "Yarlung Tsangpo", both of which are acceptable since they are transliterated from Tibetan language (also mentioned in Abstract).

Change: There is no relevant change in the manuscript.

An integration of gauge, satellite and reanalysis precipitation datasets

for the largest river basin of the Tibetan Plateau

Yuanwei Wang[1,3], Lei Wang[1,2,3*], Xiuping Li[1,2], Jing Zhou[1], Zhidan Hu[4]

[1] Key Laboratory of Tibetan Environmental Changes and Land Surface Processes,

Institute of Tibetan Plateau Research, Chinese Academy of Sciences, Beijing, China

[2] CAS Center for Excellence in Tibetan Plateau Earth Sciences, Beijing, China

[3] University of Chinese Academy of Sciences, Beijing, China

[4] Information Center, Ministry of Water Resources, Beijing, China

Corresponding author:

Lei Wang, Dr., Prof.

Key Lab. of Tibetan Environmental Changes and Land Surface Processes,

Institute of Tibetan Plateau Research, Chinese Academy of Sciences

No. 16 Lincui Road, Chaoyang District, Beijing 100101, China

Tel: +86-10-84097107   Fax: +86-10-84097079

Email: wanglei@itpcas.ac.cn

Abstract: As the largest river basin of the Tibetan Plateau, the Upper Brahmaputra River Basin (also called "Yarlung Zangbo" in Chinese) has profound impacts on the water security of local and downstream inhabitants. Precipitation in the basin is mainly controlled by the Indian Summer Monsoon and Westerly, and is the key to understand the water resources available in the basin; however, due to sparse observational data constrained by a harsh environment and complex topography, there remains a lack of reliable information on basin-wide precipitation (there are only nine national meteorological stations with continuous observations). To improve the accuracy of basin-wide precipitation data, we integrate various gauge, satellite and reanalysis precipitation datasets, including GLDAS, ITP-Forcing, MERRA2, TRMM and CMA datasets, to develop a new precipitation product for the 1981-2016 period over the Upper Brahmaputra River Basin, at 3-hour and 5-km resolution. The new product has been rigorously validated at different temporal scales (e.g. extreme events, daily to monthly variability, and long-term trends) and spatial scales (point- and basin-scale) with gauge precipitation observations, showing much improved accuracies compared to previous products. An improved hydrological simulation has been achieved (low relative bias: -5.94%; highest NSE: 0.643) with the new precipitation inputs, showing reliability and potential for multi-disciplinary studies. This new precipitation product is openly accessible at https://doi.org/10.5281/zenodo.3711155 (Wang et al., 2020) and, additionally at the National Tibetan Plateau Data Center (https://data.tpdc.ac.cn, login required).

1. Introduction

Precipitation plays a very important role in the research of hydrology, meteorology, ecology, and even social economics, as it is a critical input factor for various models (e.g. hydrological and land surface models) (Qi et al., 2016; Wang et al., 2017a; Fang et al., 2019; Miri et al., 2019; Wang et al., 2019a). Specifically, precipitation is a key part of the water balance and energy cycle and will directly impact runoff generation and soil moisture movement (Su et al., 2008). As a result, water resource management tasks such as flood forecasting and drought monitoring, ecological environment restoration (e.g. vegetation growth and protection), and many other scientific and social applications are closely linked with precipitation patterns (Funk et al., 2015).

The Tibetan Plateau (TP), known as the highest plateau in the world, is covered by massive glaciers, snow and permafrost, which significantly affect the hydrological processes of all the large rivers that are fed by it; the Brahmaputra, the Salween, and the Mekong, among others. Therefore, it is necessary to explore the hydrological variations over the TP to achieve efficient utilization and protection of its water resources and a better understanding of the effects of climate change on the surrounding region. However, due to the irregular and sparse distribution of national meteorological stations, particularly in the Upper Brahmaputra (precipitation data from only nine stations are available, and are sparsely distributed; see Sang et al., 2016; Cuo et al., 2019), there are large data constraints on research on these hydrological processes and their responses to climate change. Although there are many more rain gauges managed by the Ministry of Water Resources (MWR), most

67 of them are located in middle-stream regions and rainfall datasets are only recorded

68 over short time periods. Simply using the linear mean of these station observations to

69 calculate variations in precipitation for the entire basin is impractical and prone to

70 problems (Lu et al., 2015). Accurate spatial distributions of precipitation are

71 unavailable. This influences the generation of historical runoff data (Mazzoleni et al.,

72 2019), meaning that the specific contributions of glaciers, snow cover, permafrost and

73 vegetation to hydrological processes in this area cannot be analyzed and quantified,

74 posing a threat to regional sustainable development and living conditions (Shen et al.,

75 2010; Guo et al., 2016; Kidd et al., 2017; Shi et al., 2017; Ruhi et al., 2018; Sun et al.,

76 2018).

77   A longer time series of spatially consistent and temporally continuous

78 precipitation products could be used to improve our understanding of feedback

79 mechanisms between different meteorological and hydrological components,

80 especially under the background signal of climate change. Various satellite rainfall

81 products have been widely used in previous studies, such as the National Oceanic and

82 Atmospheric Administration/Climate Prediction Centre (NOAA/CPC) morphing

83 technique (CMORPH) (Ferraro et al., 2000; Joyce et al., 2004), and the Tropical

84 Rainfall Measuring Mission (TRMM) (Huffman et al., 2007). However, there are still

85 problems in estimating daily (Meng et al., 2014; Bai and Liu, 2018) and extreme

86 precipitation (Funk et al., 2015; Zhou et al., 2015b; Fang et al., 2019), especially in

87 mountainous regions with high elevations and fewer ground measurements, such as

88 the Upper Brahmaputra (Xia et al., 2015; Xu et al., 2017; Qi et al., 2018). Additionally,

89   there are several reanalysis datasets that have been widely used by researchers, such

90   as the Global Land Data Assimilation System (GLDAS) (Rodell et al., 2004; Zaitchik

91   et al., 2010; Wang et al., 2011) and the Modern-Era Retrospective analysis for

92   Research and Applications, Version 2 (MERRA2) dataset (Gelaro et al., 2017; Reichle

93   et al., 2017a, 2017b). Evaluation of GLDAS data has generally been limited to the

94   United States and other regions with adequate ground observations (Kato et al., 2007;

95   Qi et al., 2016). Most studies have focused on evapotranspiration, soil moisture and

96   groundwater products derived from GLDAS or MERRA2 (Bibi et al., 2019; Deng et

97   al., 2019; Li et al., 2019a); meanwhile, to the best of our knowledge, there has been

98   less focus on the evaluation of methods of precipitation estimation and little work on

99   the corresponding river discharge simulations within the Upper Brahmaputra River

100   Basin. These precipitation products generally have the advantage of wide and

101   consistent coverage and have shown great potential in many applications (Li et al.,

102   2015; Zhang et al., 2017; Fang et al., 2019), but also suffer from large uncertainties

103   over the Upper Brahmaputra River Basin due to indirect observations, insufficient

104   gauge calibration, and complex topography (Tong et al., 2014; Yong et al., 2015; Xu

105   et al., 2017).

106   In this study, we focus on integrating gauge, satellite and reanalysis precipitation

107   datasets to generate a new dataset over the Upper Brahmaputra, suitable for use in

108   hydrological simulations and other scientific researches related to climate change. The

109   remainder of this study is structured as follows. Section 2 briefly describes the study

110   area, datasets, and methodology used. Section 3 presents and discusses the evaluation

111 results of different products and validates the accuracy and reliability of our integrated

112 dataset. Then Section 4 is the data availability. Finally, conclusions are given in

113 Section 5.

114 **2. Materials and Methods**

115 **2.1. Study Area**

116   This study is conducted in Upper Brahmaputra River Basin (27°-32°N, 81°-98°E)

117 located in the south of the Tibetan Plateau (Figure 1). The Brahmaputra River is an

118 important part of the whole GBM basin (Ganges, Brahmaputra, Meghna) which

119 significant influences the natural resources and social development of the Tibetan

120 Plateau and South Asia. The river is approximately 2,057 km long with a drainage

121 area of 240,000 km^2. The climatic conditions are complicated by the extremely high

122 altitude and highly varying topography (Wang et al., 2018; Wang et al., 2019b);

123 elevation varies by up to 6,500 m throughout the study region. Generally, the

124 intra-annual distribution of precipitation is extremely uneven, with more precipitation

125 distributed in the warm seasons (Wang et al., 2019a). Since the Indian and East Asian

126 monsoons bring more water vapor in summer and the westerlies dominate in winter

127 (Yi et al., 2013; Wang et al., 2018; Li et al., 2019a, 2019b), there is a declining trend

128 of precipitation from the humid southeast to the arid northwest, on average. In recent

129 decades, the TP has been experiencing a significant warming trend exceeding that in

130 the Northern Hemisphere (Liu and Chen, 2000; Yang et al., 2014), which will affect

131 the generation and distribution of precipitation and influence hydrological processes

132 throughout the Upper Brahmaputra.

2.2. Datasets

Monthly precipitation data (1981-2016) from nine meteorological stations were obtained from the China Meteorological Administration (CMA), and daily precipitation data (May to October in 2014 and 2016) from166 rain gauges were accessed through the Ministry of Water Resources (MWR), China (Figure 1). Both of these are regarded as observed precipitation data. Daily river discharge data at Nuxia station (Figure 1) are used to assess the simulation performance when forced by different precipitation products.

In this study, we chose five types of satellite and reanalysis precipitation products (Table 1). We, first, evaluated their performance at detecting precipitation, and second, integrated them to generate a better product, designed to enhance the strengths of each product.

The three satellite and reanalysis data products, GLDAS, MERRA2 and TRMM, were acquired from the National Aeronautics and Space Administration (NASA) website (https://disc.gsfc.nasa.gov/). GLDAS ingests satellite- and ground-based observational data products and applies advanced land surface modeling and data assimilation techniques (Rodell et al., 2004; Zaitchik et al., 2010; Xia et al., 2019); it has been widely used for river discharge simulations, groundwater monitoring and many other fields (Wang et al., 2011; Chen et al., 2013; Qi et al., 2018; Verma and Katpatal, 2019). MERRA2 is the first long-term global reanalysis dataset to assimilate space-based observations of aerosols and represent their interactions alongside other physical processes in the climate system (Marquardt Collow et al., 2016; Reichle et al.,

155 2017a, 2017b), and TRMM is a joint mission between the NASA and the Japan

156 Aerospace Exploration Agency (JAXA) to study rainfall for weather and climate

157 research (Xu et al., 2017; Ali et al., 2019; Wang et al., 2019a). The ITP-Forcing

158 dataset has been developed by the hydrometeorological research group at the Institute

159 of Tibetan Plateau Research, Chinese Academy of Sciences (He, 2010), and has been

160 shown to perform well on the TP (Yang et al., 2010; Chen et al., 2011). These data

161 were downloaded from the Cold and Arid Regions Science Data Center

162 (http://westdc.westgis.ac.cn/).

163 **2.3. Methods**

164   In this study, because of the different spatial resolutions of different products, we

165 extracted the precipitation values from each product according to the locations of the

166 gauges to generate product-gauge data pairings for evaluation. Where there are at least

167 two gauges in the pixel of one product, we used the average value of the gauges to

168 evaluate the performance of the corresponding precipitation product data.

169   To ensure the consistency of different products, we interpolated all the products

170 into the same 5 km spatial resolution grid using the inverse distance weighted (IDW)

171 method (Ma et al., 2019; Qiao et al., 2019; Sangani et al., 2019) and calculated them

172 at 3-hourly resolution. Due to its good performance on the TP, we then used the

173 ITP-Forcing data (1981-2016) to derive the multi-year mean 3-hour data as

174 background climatological precipitation. Then, the precipitation anomalies between

175 CMA, GLDAS, ITP-Forcing, MERRA2, TRMM and the background were calculated

176 3-hourly, using:

$$\varepsilon_c = P_C - P_B$$
$$\varepsilon_g = P_G - P_B$$
177
$$\varepsilon_i = P_I - P_B \tag{1}$$
$$\varepsilon_m = P_M - P_B$$
$$\varepsilon_t = P_T - P_B$$

178 where P_B, P_C, P_G, P_I, P_M, P_T represent the background precipitation and different

179 products, respectively, and ε denotes the corresponding precipitation anomalies.

180 Considering different weights for these anomalies, we combined the background

181 precipitation with these anomalies,

182
$$P\_int = P_B + w_1\varepsilon_c + w_2\varepsilon_g + w_3\varepsilon_i + w_4\varepsilon_m + w_5\varepsilon_t \tag{2}$$

183 where w represents the weight for each anomaly and P_int refers to the new integrated

184 precipitation at 5 km and 3-hourly resolution.

185   After P_int was acquired, we corrected its probability distribution function (PDF)

186 based on the rain gauges, and undertook several validation steps for spatial

187 distribution and at different time scales (e.g. extreme events, seasonal to inter-annual

188 variability, and long-term trends). At the same time, we also analyzed the changing

189 trend over the 36 years, and the extremely high precipitation events during the warm

190 months in 2014 and 2016. In order to identify the extreme events, we first assumed

191 that daily precipitation conforms to a normal distribution. From this we calculated a

192 threshold, above which the probability of precipitation values occurring is less than

193 0.05 (e.g. Fang et al., 2019 use 0.1). We considered events with precipitation values

194 above this threshold as extreme events.

195
$$P\left(precipitation \geq threshold \right) \leq 0.05 \tag{3}$$

196 where P denotes the probability. Finally, based on the observed discharge data at

197   Nuxia Station, we compared the simulated daily discharges (normalized) from 2008 to

198   2016 using a water and energy budget-based distributed hydrological model

199   (WEB-DHM) to check the accuracy and reliability of our integrated precipitation.

200   Evaluation criteria used in the discharge error assessment include relative bias (RB)

201   and the Nash-Sutcliffe coefficient of efficiency (NSE).

$$Q_{normalized} = \frac{Q - \min Q_{obs}}{\max Q_{obs} - \min Q_{obs}} \tag{4}$$

$$RB = \frac{\sum_{i=1}^{n} Q_{sim} - \sum_{i=1}^{n} Q_{obs}}{\sum_{i=1}^{n} Q_{obs}} \times 100\% \tag{5}$$

$$NSE = 1 - \frac{\sum_{i=1}^{n} \left(Q_{obs} - Q_{sim}\right)^2}{\sum_{i=1}^{n} \left(Q_{obs} - \overline{Q_{obs}}\right)^2} \tag{6}$$

205   Where $Q_{normalized}$, Q_{obs}, Q_{sim} represent the normalized discharge, observed discharge,

206   and simulated discharge, respectively. The perfect value of *RB* is 0 and that of *NSE* is

207   1. More information about this model can be found in many studies (Wang et al., 2009;

208   Wang and Koike, 2009; Xue et al., 2013; Zhou et al., 2015a; Wang et al., 2016; Wang

209   et al., 2017a). Figure 2 shows the flowchart of this study and Figure 3 presents the

210   final spatial distribution of our integrated product.

211   **3. Results and Discussion**

212   **3.1. Evaluation of precipitation products at the basin and grid scale**

213   Figures 4 and 5 analyze the overall regime of different precipitation products at

214   the basin scale. Figure 4 is the spatial distribution in warm (May to Oct.) and cold

215   (Nov. to Apr.) months, and Figure 5 presents the time series of basin-averaged annual

216   and monthly precipitation values. The spatial pattern indicates that more precipitation

217   occurs in warm seasons and less in cold seasons. During the warm months, GLDAS

218   and TRMM present obvious regional differences between upstream and downstream,

219   while CMA gridded data show the lesser values in the upstream source region. In the

220   cold seasons, all products present almost the same pattern, among which MERRA2

221   gives the lowest precipitation values.

222   For annual precipitation, CMA, ITP-Forcing and MERRA2 show similar

223   characteristics (annual mean value: 615 mm, 550 mm and 506 mm, respectively),

224   while GLDAS and TRMM are 789 mm and 757 mm, respectively. There are also

225   significant ($p < 0.01$) increasing trends in annual precipitation of GLDAS,

226   ITP-Forcing, and MERRA2 (6.42, 3.28, 4.68 mm/year, respectively) over the 36 years

227   of the data. For monthly precipitation, GLDAS and TRMM greatly overestimate

228   summer precipitation compared to the others, which explains why these two products

229   give anomalously high annual values (nearly 200 mm greater than the other three data

230   products). On the other hand, the monthly variations indicate that the intra-annual

231   distribution of precipitation is extremely uneven.

232   Figures 6 and 7 compare the accuracy of monthly rainfall from different products

233   at the grid scale. Due to the coarse spatial resolution of MERRA2 (0.5°×0.625°), there

234   are fewer product-gauge data pairings available for evaluation. All the products show

235   similar correlation relationships with the observations, with most rain gauges

236   overestimating monthly precipitation (Figure 7). The highest correlation coefficient is

237 0.63 (MERRA2) and the lowest is 0.51 (GLDAS). The PDFs, however, show

238 different characteristics (Figure 6). The CMA data are more consistent with the gauge

239 data, while GLDAS and TRMM exhibit clear overestimations. As for ITP-Forcing, its

240 precipitation is more concentrated on the average value, as indicated by the narrow

241 curve.

3.2. Integration of precipitation products and validation of *P_int*

3.2.1. Integration of precipitation products and validation against different time

series

245 Figure 3 presents the spatial distribution of annual and seasonal precipitation

246 estimated by our integrated dataset, which shows a declining trend from the southeast

247 to northwest. Figure 5 then compares the monthly and annual precipitation calculated

248 from our integrated dataset with the satellite and reanalysis products. As discussed in

249 Section 2.3, we interpolated all the products into a spatial resolution of 5 km using the

250 IDW method, and calculated them at a temporal resolution of 3 hours. Comparing

251 different weights for the anomalies mentioned in Equation 2, we finally adopted the

252 same weight for each product and the sum of the weights is 1 (w = 1/3 from 1981 to

253 1997; w = 0.25 from 1998 to 2007; w = 0.2 from 2008 to 2016) to develop the new

254 product. We made the integrated precipitation data using equal weights essentially

255 according to the number of available precipitation products at different time periods

256 (Table 1). Then we corrected the PDF of the newly integrated data based on the rain

257 gauge observations (Figure 6).

258 After *P_int* was derived, we first validated its performance against short time

259 series (Figure 8). *P_int* shows optimal performance at detecting daily precipitation

260 with the correlation coefficients of 0.43 in 2014 and 0.55 in 2016. In 2014, the

261 average bias is 0.20 mm and the root mean square error (RMSE) is 4.18 mm. *P_int*

262 successfully captures the daily variation of precipitation except for late September and

263 early October. For 2016, the average bias and RMSE are -0.006 mm and 2.62 mm,

264 respectively, much better than those for 2014.

265 We then check the spatial distribution of *P_int* from May to October in 2014 and

266 2016 (Figure 9). Every rain gauge is compared with its corresponding grid in *P_int* to

267 explore the spatial heterogeneity. *P_int* well reproduces the precipitation pattern

268 described by less rain in the upstream (western) regions and more rain in the

269 downstream (eastern) regions. Meanwhile, abundant rainfall occurs in summer,

270 particularly for July.

271 Building on this, further validation was undertaken against a long time series. We

272 chose the average monthly precipitation from the nine meteorological stations as the

273 evaluation standard against which to assess *P_int* (Figure 10). The PDF of *P_int* is

274 consistent with that of the station data, which indicates that the mean value and

275 standard deviation of *P_int* are much closer to the observed value (Figure 10a).

276 Similar to the short time series, the average bias (-4.50 mm) and the RMSE (13.6 mm),

277 especially with respect to the correlation coefficient (0.96), prove that the *P_int* is

278 applicable and reliable.

279 **3.2.2. Trend and extreme events analysis compared across different precipitation**

280 **products**

281   The trend analysis (Figure 11) over 36 years indicates that there are different

282   patterns of precipitation in different seasons and different regions. In summer, there

283   are more complicated trends, as the variations between up and down stream differ

284   greatly. On the contrary, trends of winter precipitation values over most of the study

285   region vary by merely ±2 mm/year, illustrating that precipitation in winter generally

286   remains unchanged or experiences minimal change. To find if *P_int* is able to reflect

287   the true varying trend, we added a comparison between meteorological stations

288   (triangles in Figure 11 and their direction represent the true trend) and precipitation

289   products. For observed annual precipitation, all the stations give an insignificant

290   increasing trend, except for Bomi station, which is located in the easternmost part of

291   the study region. For seasonal precipitation, different stations present different

292   patterns. As a result, *P_int* appears to reflect the changing pattern of more stations

293   than any other product, with the exception of the ITP-Forcing dataset on an annual

294   timescale or over autumn (Figure 12).

295   We notice that there is increasing trend in annual precipitation almost in the

296   whole basin for *P_int*; only precipitation in the midstream area near the Himalaya

297   mountains and small part of the upstream region are decreasing. Moreover, the

298   majority of the increased precipitation in the downstream regions occurs over spring

299   and summer, with only slight changes found in autumn and winter.

300   After the volume, the spatial distribution, and the trend of *P_int* at different time

301   scales were completely verified, we continued to inspect if *P_int* could capture the

302   extreme events from May to October in 2014 and 2016 according to the rain gauge

303   data (Figure 13). There are 27 days in total (19 days in 2014 and 8 days in 2016)

304   when extremely high daily precipitation occurred. All the products are comparable

305   with each other in underestimating the frequency of extreme events. Nine days are

306   identified out of the *P_int* data, lesser only to the number of days detected by

307   ITP-Forcing (11 days).

308   **3.2.3. Evaluation of daily discharges simulated by different precipitation**

309   **products**

310   All the comparison and validation steps undertaken above support the accuracy

311   and reliability of our integrated dataset. Furthermore, Figure 14 indicates the superior

312   suitability and application of *P_int* in hydrological simulation and investigation, with

313   an RB of -5.94% and an NSE of 0.643 (the highest). We simulate the daily discharge

314   of Nuxia station using the various precipitation datasets as the input with the same

315   initial conditions and physical parameters. All products overestimate the daily

316   discharge, except for *P_int* (-5.94%) and MERRA2 (-2.24%). In terms of NSE, *P_int*

317   (0.643), ITP-Forcing (0.543) and MERRA2 (0.544) are higher than others, explaining

318   their better simulation performance. GLDAS and TRMM offer the worst performance

319   in discharge simulation, which is consistent with their overestimation of precipitation

320   in summer (Figure 5). This indicates that these datasets should be corrected when

321   undertaking hydrological research over the Upper Brahmaputra.

322   **4. Data availability**

323   This high spatiotemporal resolution (5km, 3h) precipitation dataset over the

324   Upper Brahmaputra River Basin from 1981 to 2016 is freely available at

325 https://doi.org/10.5281/zenodo.3711155 (Wang et al., 2020), which can be

326 downloaded in TXT format.

327 **5. Conclusion**

328   In order to acquire suitable and accurate precipitation datasets which are helpful

329 in hydrology, meteorology and other scientific research over the Upper Brahmaputra,

330 we produced a new precipitation product by integrating gauge, satellite and reanalysis

331 precipitation datasets to reduce the uncertainties associated with a single product and

332 limitation of few observation stations. Our integrated dataset performs better than the

333 input datasets in estimating daily and monthly precipitation, describing the spatial

334 heterogeneity, capturing variation trends and extreme events and simulating river

335 discharges. Furthermore, it is successful in reproducing daily precipitation variation,

336 with smaller average biases (0.2 mm in 2014 and -0.006 mm in 2016) and RMSE

337 values (4.18 mm in 2014 and 2.62 mm in 2016). Monthly precipitation shows higher

338 correlation coefficients with the in-situ data for various time series (0.69 for all the

339 rain gauges in the warm months of 2014 and 2016; 0.86 for the nine meteorological

340 stations over 1981-2016). This high spatio-temporal resolution assures us that we can

341 use this new dataset to explore more detailed physical processes and further

342 understand the impacts of climate change on the water resources of the Upper

343 Brahmaputra River Basin, and we are confident that our precipitation dataset will

344 greatly assist future research in this basin.

345   With this in mind, we note some aspects of this study that deserve further

346 consideration. The effect of altitude on precipitation has not been taken into account

347 in the development of this dataset. The 166 rain gauges used in this paper, are all

348 located at the elevations above 3500 m, except for several eastern gauges. Generally,

349 these gauges were installed at relatively plain area, which may lead to large

350 uncertainty in estimating precipitation (rain or snow) at high mountains, especially in

351 the daily or finer time scales (Ahrens, 2006; Haiden and Pistotnik, 2009). This

352 limitation can be even more severe, due to the orographic effect on precipitation rates,

353 in mountainous regions and transition zones between the low and high altitudes,

354 which will result in the underestimates of the actual basin-wide precipitation (Anders

355 et al., 2006; Hashemi et al., 2020). Increasing the density and the distribution area of

356 observational stations can directly weaken this altitude effects. We also note

357 uncertainties that may arise from the re-gridding of the remotely sensed datasets in

358 order to pair with the in-situ gauge data. In addition, the assumption of normal

359 distribution when analyzing extremely high daily precipitation can also lead to

360 uncertainty. Generally, the non-normal (skewed) distribution of precipitation is caused

361 by the zero rainfall events at single site (Kumar et al., 2009; Semenov, 2008;

362 Sloughter et al., 2007). An associated problem is the quantity and reliability of the

363 data used to fit the distribution. Different probability distributions are used to describe

364 the observed time series of daily precipitation, then different extreme values may be

365 obtained (Angelidis et al., 2012). This study provides a foundation from which further

366 studies can be carried out to explore these aspects in more detail.

367   In the future, more studies are needed to validate the method and data in regions

368 with complex topography and climatic conditions, and to further improve the retrieval

369 algorithm. This will greatly benefit hydrological applications, especially in areas with

370 sparse and irregular observation networks. Furthermore, no products used in this

371 study accurately represent extreme precipitation events, thus, it is necessary to

372 improve the ability of all of these products to capture extreme events.

373 **Acknowledgments**

374 This study was financially supported by the National Natural Science Foundation

375 of China (Grant No. 91747201) and the Strategic Priority Research Program of

376 Chinese Academy of Sciences (Grant No. XDA20060202 and XDA19070301). Jing

377 Zhou was supported by the National Natural Science Foundation of China (Grant No.

378 41771089). The Shuttle Radar Topographic Mission (SRTM) Digital Elevation Model

379 (DEM), with a ground resolution of 30 m, is available from the United States

380 Geological Survey's (USGS) web portal (www.earthexplorer.usgs.gov). We would

381 also like to thank NASA for different precipitation data including GLDAS, MERRA2,

382 TRMM (https://disc.gsfc.nasa.gov/). Lastly, we are pleased to acknowledge the

383 anonymous reviewers and editor's valuable comments and suggestions to improve

384 this manuscript.

385 **Conflicts of Interest**

386 The authors declare no conflicts of interest.

387 **References**

388 Ahrens, B.: Distance in spatial interpolation of daily rain gauge data. Hydrol. Earth

389 Syst. Sci., 10, 197-208, 2006.

390 Ali, S., Tong, D., Xu, Z., Henchiri, M., Wilson, K., Shi, S., and Zhang, J.:

391   Characterization of drought monitoring events through MODIS- and

392   TRMM-based DSI and TVDI over south Asia during 2001–2017, Environ. Sci.

393   Pollut. Res., 26(32), 33568-33581, 2019.

394   Anders, A.M., Roe, G.H., Hallet, B., Montgomery, D.R., and Putkonen, J.: Spatial

395   patterns of precipitation and topography in the himalaya. Geol. Soc. Am. Spec.

396   Pap., 398, 39-53, 2006.

397   Angelidis, P., Maris, F., Kotsovinos, N., and Hrissanthou, V.: Computation of

398   Drought Index SPI with Alternative Distribution Functions. Water Resour.

399   Manage., 26(9), 2453-2473, 2012.

400   Bai, P., and Liu, X.: Evaluation of Five Satellite-Based Precipitation Products in Two

401   Gauge-Scarce Basins on the Tibetan Plateau, Remote Sens., 10(8), 1316, 2018.

402   Bibi, S., Wang, L., Li, X., Zhang, X., and Chen, D.: Response of groundwater storage

403   and recharge in the Qaidam Basin (Tibetan Plateau) to climate variations from

404   2002 to 2016, J. Geophys. Res.: Atmos., 124(17-18), 9918-9934, 2019.

405   Chen, Y., Yang, K., He, J., Qin, J., Shi, J., Du, J., and He, Q.: Improving land surface

406   temperature modeling for dry land of China, J. Geophys. Res.: Atmos., 116(D20),

407   2011.

408   Chen, Y., Yang, K., Qin, J., Zhao, L., Tang, W., and Han, M.: Evaluation of AMSR-E

409   retrievals and GLDAS simulations against observations of a soil moisture

410   network on the central Tibetan Plateau, J. Geophys. Res.: Atmos., 118(10),

411   4466-4475, 2013.

412   Cuo, L., Li, N., Liu, Z., Ding, J., Liang, L., Zhang, Y., and Gong, T.: Warming and

413   human activities induced changes in the Yarlung Tsangpo basin of the Tibetan

414   plateau and their influences on streamflow, J. Hydrol.: Regional Studies, 25,

415   100625, 2019

416   Deng, M., Meng, X., Li, Z., Lyv, Y., Lei, H., Zhao, L., Zhao, S., Ge, J., and Jing, H.:

417   Responses of soil moisture to regional climate change over the Three Rivers

418   Source Region on the Tibetan plateau, Int. J. Climatol., 1-15, 2019.

419   Fang, J., Yang, W., Luan, Y., Du, J., Lin, A., and Zhao, L.: Evaluation of the TRMM

420   3B42 and GPM IMERG products for extreme precipitation analysis over China,

421   Atmos. Res., 223, 24-38, 2019.

422   Ferraro, R.R., Weng, F., Grody, N.C., and Zhao, L.: Precipitation characteristics over

423   land from the NOAA−15 AMSU sensor, Geophys. Res. Lett., 27(17), 2669-2672,

424   2000.

425   Funk, C., Peterson, P., Landsfeld, M., Pedreros, D., Verdin, J., Shukla, S., Husak, G.,

426   Rowland, J., Harrison, L., Hoell, A., and Michaelsen, J.: The climate hazards

427   infrared precipitation with stations-a new environmental record for monitoring

428   extremes, Sci. Data, 2(1), 1-21, 2015.

429   Gelaro, R., McCarty, W., Suárez, M.J., Todling, R., Molod, A., Takacs, L., Randles,

430   C.A., Darmenova, A., Bosilovicha, M.G., Reichlea, R., Wargan, K., Coya, L.,

431   Cullather, R., Draper, C., Akella, S., Buchard, V., Conaty, A., Silva, A.M., Gu,

432   W., Kima, G-K., Koster, R., Lucchesi, R., Merkova, D., Nielsen, J.E., Partyka,

433   G., Pawsona, S., Putman, W., Rienecker, M., Schubert, S.D., Sienkiewicz, M.,

434   and Zhao, B.: The modern-era retrospective analysis for research and

435 applications, version 2 (MERRA-2), J. Clim., 30(14), 5419-5454, 2017.

436 Guo, H., Chen, S., Bao, A., Behrangi, A., Hong, Y., Ndayisaba, F., Hu, J., and

437   Stepanian, P.M.: Early assessment of integrated multi-satellite retrievals for

438   global precipitation measurement over China, Atmos. Res., 176, 121-133, 2016.

439 Haiden, T., and Pistotnik, G.: Intensity-dependent parameterization of elevation

440   effects in precipitation analysis. Adv. Geosci., 33-38, 2009.

441 Hashemi, H., Fayne, J.V., Lakshmi, V., and Huffman, G.J.: Very high resolution,

442   altitude-corrected, TMPA-based monthly satellite precipitation product over the

443   CONUS. Sci. Data, 7(1), 2020.

444 He, J.: Development of surface meteorological dataset of China with high temporal

445   and spatial resolution, Master dissertation, Institute of Tibetan Plateau Research,

446   Chinese Academy of Science, 2010.

447 Huffman, G.J., Adler, R.F., Rudolf, B., Schneider, U., and Keehn, P.R.: Global

448   precipitation estimates based on a technique for combining satellite-based

449   estimates, rain gauge analysis, and NWP model precipitation information, J.

450   Clim., 8(5), 1284-1295, 1995.

451 Huffman, G.J., Bolvin, D.T., Nelkin, E.J, Wolff, D.B., Adler, R.F., Gu, G., Hong, Y.,

452   Bowman, K.P., and Stocker, E.F.: The TRMM multisatellite precipitation

453   analysis (TMPA): Quasi-global, multiyear, combined-sensor precipitation

454   estimates at fine scales, J. Hydrometeorol., 8(1), 38-55, 2007.

455 Joyce, R.J, Janowiak, J.E., Arkin, P.A., and Xie, P.: CMORPH: A method that

456   produces global precipitation estimates from passive microwave and infrared

457  data at high spatial and temporal resolution, J. Hydrometeorol., 5(3), 487-503,

458  2004.

459 Kato, H., Rodell, M., Beyrich, F., Cleugh, H., Gorsel, E.V., Liu, H., and Meyers, T.P.:

460  Sensitivity of land surface simulations to model physics, land characteristics, and

461  forcings, at four CEOP sites, J. Meteorol. Soc. Jpn., 85, 187-204, 2007.

462 Kidd, C., Becker, A., Huffman, G.J., Muller, C.L., Joe, P., Skofronick-Jackson, G.,

463  and Kirschbaum, D.B.: So, how much of the Earth's surface is covered by rain

464  gauges?, Bull. Am. Meteorol. Soc., 98(1), 69-78, 2017.

465 Kumar, M.N., Murthy, C.S., Sai, M.V., and Roy, P.S.: On the use of Standardized

466  Precipitation Index (SPI) for drought intensity assessment. Meteorol. Appl.,

467  16(3), 381-389, 2009.

468 Li, X., Long, D., Han, Z., Scanlon, B.R., Sun, Z., Han, P., and Hou, A.:

469  Evapotranspiration Estimation for Tibetan Plateau Headwaters using Conjoint

470  Terrestrial and Atmospheric Water Balances and Multisource Remote Sensing,

471  Water Resour. Res., 55, https://doi.org/10.1029/2019WR025196, 2019a.

472 Li, X., Long, D., Huang, Q., Han, P., Zhao, F., and Wada, Y.:

473  High-temporal-resolution water level and storage change data sets for lakes on

474  the Tibetan Plateau during 2000–2017 using multiple altimetric missions and

475  Landsat-derived lake shoreline positions, Earth Syst. Sci. Data, 11(4), 1603-1627,

476  2019b.

477 Li, Z., Yang, D., Gao, B., Jiao, Y., Hong, Y., and Xu, T.: Multiscale hydrologic

478  applications of the latest satellite precipitation products in the Yangtze River

479   Basin using a distributed hydrologic model, J Hydrometeorol., 16(1), 407-426,

480   2015.

481   Liu, X., and Chen, B.: Climatic warming in the Tibetan Plateau during recent decades,

482   Int. J. Climatol., 20(14), 1729-1742, 2000.

483   Lu, N., Trenberth, K.E., Qin, J., Yang, K., and Yao, L.: Detecting long-term trends in

484   precipitable water over the Tibetan Plateau by synthesis of station and MODIS

485   observations, J. Clim., 28(4), 1707-1722, 2015.

486   Ma, J., Ding, Y., Cheng, J.C.P., Jiang, F., and Wan, Z.: A temporal-spatial

487   interpolation and extrapolation method based on geographic Long Short-Term

488   Memory neural network for PM 2.5, J. Cleaner Prod., 237, 117729, 2019.

489   Marquardt Collow, A.B., Bosilovich, M.G., and Koster, R.D.: Large-scale influences

490   on summertime extreme precipitation in the northeastern United States, J.

491   Hydrometeorol., 17(12), 3045-3061, 2016.

492   Mazzoleni, M., Brandimarte, L., and Amaranto, A.: Evaluating precipitation datasets

493   for large-scale distributed hydrological modelling, J. Hydrol., 578, 124076, 2019.

494   Meng, J., Li, L., Hao, Z., Wang, J., and Shao, Q.: Suitability of TRMM satellite

495   rainfall in driving a distributed hydrological model in the source region of

496   Yellow River, J. Hydrol., 509, 320-332, 2014.

497   Miri, M., Masoudi, R., and Raziei, T.: Performance Evaluation of Three

498   Satellites-Based Precipitation Data Sets Over Iran, J. Indian Soc. Remot., 47(12),

499   2073-2084, 2019.

500   Qi, W., Liu, J., and Chen, D.: Evaluations and improvements of GLDAS2.0 and

501   GLDAS2.1 forcing data's applicability for basin scale hydrological simulations

502   in the Tibetan Plateau, J. Geophys. Res.: Atmos., 123(23), 13,128-13,148, 2018.

503   Qi, W., Zhang, C., Fu, G., Sweetapple, C., and Zhou, H.: Evaluation of global

504   fine-resolution precipitation products and their uncertainty quantification in

505   ensemble discharge simulations, Hydrol. Earth Syst. Sci., 20(2), 903-920, 2016.

506   Qi, W., Zhang, C., Fu, G., and Zhou H.: Global Land Data Assimilation System data

507   assessment using a distributed biosphere hydrological model, J. Hydrol., 528,

508   652-667, 2015.

509   Qiao, P., Li, P., Cheng, Y., Wei, W., Yang, S., Lei, M., and Chen, T.: Comparison of

510   common spatial interpolation methods for analyzing pollutant spatial

511   distributions at contaminated sites, Environ. Geochem. Health, 41, 2709-2730,

512   2019.

513   Rasouli, K., Pomeroy, J.W., Janowicz, J.R., Williams, T.J., and Carey, S.K.: A

514   long-term hydrometeorological dataset (1993–2014) of a northern mountain

515   basin: Wolf Creek Research Basin, Yukon Territory, Canada, Earth Syst. Sci.

516   Data, 11(1), 89-100, 2019.

517   Reichle, R.H., Draper, C.S., Liu, Q., Girotto, M., Mahanama, S.P.P., Koster, R.D.,

518   and De Lannoy, G.J.M.: Assessment of MERRA-2 land surface hydrology

519   estimates, J. Clim., 30(8), 2937-2960, 2017a.

520   Reichle, R.H., Liu, Q., Koster, R.D., Draper, C.S., Mahanama, S.P.P., and Partyka,

521   G.S.: Land surface precipitation in MERRA-2, J. Clim., 30(5), 1643-1664,

522   2017b.

523 Roca, R., Alexander, L.V., Potter, G., Bador, M., Juca, R., Contractor, S., Bosilovich,

524   M.G., and Cloche, S.: FROGS: a daily 1°× 1° gridded precipitation database of

525   rain gauge, satellite and reanalysis products, Earth Syst. Sci. Data, 11(3),

526   1017-1035, 2019.

527 Rodell, M., Houser, P.R., Jambor, U., Gottschalck, J., Mitchell, K., Meng, C-J.,

528   Arsenault, K., Cosgrove, B., Radakovich, J., Bosilovich, M., Entin, J.K., Walker,

529   J.P., Lohmann, D., and Toll, D.: The Global Land Data Assimilation System,

530   Bull. Am. Meteorol. Soc., 85(3), 381-394, 2004.

531 Rodell, M., McWilliams, E.B., Famiglietti, J.S., Beaudoing, H.K., and Nigro, J.:

532   Estimating evapotranspiration using an observation based terrestrial water budget,

533   Hydrol. Processes, 25(26), 4082-4092, 2011.

534 Ruhi, A., Messager, M.L., and Olden, J.D.: Tracking the pulse of the Earth's fresh

535   waters, Nature Sustainability, 1(4), 198-203, 2018.

536 Sang, Y., Singh, V.P., Gong, T., Xu, K., Sun, F., Liu, C., Liu, W., and Chen, R.:

537   Precipitation variability and response to changing climatic condition in the

538   Yarlung Tsangpo River basin, China, J. Geophys. Res.: Atmos., 121, 8820–8831,

539   doi:10.1002/2016JD025370, 2016.

540 Sangani, M.F., Khojasteh, D.N., and Owens, G.: Dataset characteristics influence the

541   performance of different interpolation methods for soil salinity spatial mapping,

542   Environ. Monit. Assess., 191(11), 684, 2019.

543 Savtchenko, A.K., Huffman, G., and Vollmer, B.: Assessment of precipitation

544   anomalies in California using TRMM and MERRA data, J. Geophys. Res.:

545   Atmos., 120(16), 8206-8215, 2015.

546   Semenov, M.A.: Simulation of extreme weather events by a stochastic weather

547   generator. Clim. Res., 35(3), 203-212, 2008.

548   Shen, G., Chen, N., Wang, W., and Chen Z.: WHU-SGCC: a novel approach for

549   blending daily satellite (CHIRP) and precipitation observations over the Jinsha

550   River basin, Earth Syst. Sci. Data, 11(4), 1711-1744, 2019.

551   Shen, Y., Xiong, A., Wang, Y., and Xie, P.: Performance of high−resolution satellite

552   precipitation products over China, J. Geophys. Res.: Atmos., 115(D2), 2010.

553   Shen, Y., Zhao, P., Pan, Y., and Yu, J.: A high spatiotemporal gauge−satellite merged

554   precipitation analysis over China, J. Geophys. Res.: Atmos., 119(6), 3063-3075,

555   2014.

556   Shi, P., Bai, X., Kong, F., Fang, J., Gong, D., Zhou, T., Guo, Y., Liu, Y., Dong, W.,

557   Wei, Z., He, C., Yu, D., Wang, J., Ye, Q., Yu, R., and Chen, D.: Urbanization

558   and air quality as major drivers of altered spatiotemporal patterns of heavy

559   rainfall in China, Landscape Ecol., 32(8), 1723-1738, 2017.

560   Sloughter, J.M., Raftery, A.E., Gneiting, T., and Fraley, C.: Probabilistic Quantitative

561   Precipitation Forecasting Using Bayesian Model Averaging. Mon. Weather Rev.,

562   135(9), 3209-3220, 2007.

563   Smith, C.D., Yang, D., Ross, A., and Barr, A.: The Environment and Climate Change

564   Canada solid precipitation intercomparison data from Bratt's Lake and Caribou

565   Creek, Saskatchewan, Earth Syst. Sci. Data, 11(3), 1337-1347, 2019.

566   Su, F., Hong, Y., and Lettenmaier, D.P.: Evaluation of TRMM Multisatellite

567   Precipitation Analysis (TMPA) and its utility in hydrologic prediction in the La

568   Plata Basin, J. Hydrometeorol., 9(4), 622-640, 2008.

569   Sun, Q., Miao, C., Duan, Q., Ashouri, H., Soroosh, S., and Hsu, K.: A review of

570   global precipitation data sets: Data sources, estimation, and intercomparisons,

571   Rev. Geophys., 56(1), 79-107, 2018.

572   Tong, K., Su, F., Yang, D., and Hao, Z.: Evaluation of satellite precipitation retrievals

573   and their potential utilities in hydrologic modeling over the Tibetan Plateau, J.

574   Hydrol., 519, 423-437, 2014.

575   Verma, K., and Katpatal, Y.B.: Groundwater monitoring using GRACE and GLDAS

576   data after downscaling within basaltic aquifer system, Groundwater, 2019.

577   Wang, F., Wang, L., Koike, T., Zhou, H., Yang, K., Wang, A., and Li, W.: Evaluation

578   and application of a fine-resolution global data set in a semiarid mesoscale river

579   basin with a distributed biosphere hydrological model, J. Geophys. Res.: Atmos.,

580   116(D21), 2011.

581   Wang, L., and Koike, T.: Comparison of a distributed biosphere hydrological model

582   with GBHM, Annual Journal of Hydraulic Engineering-JSCE, 53, 103-108,

583   2009a.

584   Wang, L., Koike, T., Yang, K., and Yeh, P.J.: Assessment of a distributed biosphere

585   hydrological model against streamflow and MODIS land surface temperature in

586   the upper Tone River Basin, J. Hydrol., 377(1-2), 21-34, 2009b.

587   Wang, L., Sun, L., Shrestha, M., Li, X., Liu, W., Zhou, J., Yang, K., Lu, H., and Chen,

588   D.: Improving snow process modeling with satellite−based estimation of

589   near−surface−air−temperature lapse rate, J. Geophys. Res.: Atmos., 121(20),

590   12005-12030, 2016.

591   Wang, L., Zhou, J., Qi, J., Sun, L., Yang, K., Tian, L., Lin, Y., Liu, W., Shrestha, M.,

592   Xue, Y., Koike, T., Ma, Y., Li, X., Chen, Y., Chen, D., Piao, S., and Lu, H.:

593   Development of a land surface model with coupled snow and frozen soil physics,

594   Water Resour. Res., 53(6), 5085-5103, 2017a.

595   Wang, S., Liu, J., Wang, J., Qiao, X., and Zhang, J.: Evaluation of GPM IMERG

596   V05B and TRMM 3B42V7 Precipitation products over high mountainous

597   tributaries in Lhasa with dense rain gauges, Remote Sens., 11(18), 2080, 2019a.

598   Wang, Y., Chen, J., and Yang, D.: Bayesian assimilation of multiscale precipitation

599   data and sparse ground gauge observations in mountainous areas, J.

600   Hydrometeorol., 20(8), 1473-1494, 2019b.

601   Wang, Y., Wang, L., Li, X., and Chen, D.: Temporal and spatial changes in estimated

602   near−surface air temperature lapse rates on Tibetan Plateau, Int. J. Climatol.,

603   38(7), 2907-2921, 2018.

604   Wang, Y., Wang, L., Li, X., and Zhou, J.: High temporal and spatial resolution

605   precipitation data of Upper Brahmaputra River Basin (1981-2016), Zenodo,

606   http://doi.org/10.5281/zenodo.3711155, 2020.

607   Wang, Y., Yang, H., Yang, D., Qin, Y., Gao, B., and Cong, Z.: Spatial Interpolation

608   of Daily Precipitation in a High Mountainous Watershed based on Gauge

609   Observations and a Regional Climate Model Simulation, J. Hydrometeorol.,

610   18(3), 845-862, 2017b.

611   Xia, T., Wang, Z., and Zheng, H.: Topography and data mining based methods for

612   improving satellite precipitation in mountainous areas of China, Atmosphere,

613   6(8), 983-1005, 2015.

614   Xia, Y., Hao, Z., Shi, C., Li, Y., Meng, J., Xu T., Wu, X., and Zhang B.: Regional and

615   Global Land Data Assimilation Systems: Innovations, Challenges, and Prospects,

616   J. Meteorol. Res., 33(2), 159-189, 2019.

617   Xia, Y., Mocko, D.M., Wang, S., Pan, M., Kumar, S.V., Peters-Lidard, C.D., Wei, H.,

618   Wang, D., and Ek, M.B.: Comprehensive evaluation of the variable infiltration

619   capacity (VIC) model in the North American Land Data Assimilation System, J.

620   Hydrometeorol., 19(11), 1853-1879, 2018.

621   Xu, R., Tian, F., Yang, L., Hu, H., Lu, H., and Hou, A.: Ground validation of GPM

622   IMERG and TRMM 3B42V7 rainfall products over southern Tibetan Plateau

623   based on a high-density rain gauge network, J. Geophys. Res.: Atmos., 122(2),

624   910-924, 2017.

625   Xue, B., Wang, L., Yang, K., Tian, L., Qin, J., Chen, Y., Zhao, L., Ma, Y., Koike, T.,

626   Hu, Z., and Li, X.: Modeling the land surface water and energy cycles of a

627   mesoscale watershed in the central Tibetan Plateau during summer with a

628   distributed hydrological model, J. Geophys. Res.: Atmos., 118(16), 8857-8868,

629   2013.

630   Yang, K., He, J., Tang, W., Qin, J., and Chen, C.C.K.: On downward shortwave and

631   longwave radiations over high altitude regions: observation and modeling in the

632   Tibetan Plateau, Agr. Forest Meteorol., 150(1), 38-46, 2010.

633   Yang, K., Wu, H., Qin, J., Lin, C., Tang, W., and Chen, Y.: Recent climate changes

634   over the Tibetan Plateau and their impacts on energy and water cycle: A review,

635   Global Planet. Change, 112, 79-91, 2014.

636   Yi, X., Li, G., and Yin, Y.: Spatio-temporal variation of precipitation in the

637   Three-River Headwater Region from 1961 to 2010, J. Geogr. Sci., 23(3),

638   447-464, 2013.

639   Yong, B., Liu, D., Gourley, J.J., Tian, Y., Huffman, G.J., Ren, L., and Hong, Y.:

640   Global view of real-time TRMM multisatellite precipitation analysis:

641   Implications for its successor global precipitation measurement mission, Bull.

642   Am. Meteorol. Soc., 96(2), 283-296, 2015.

643   Zaitchik, B.F., Rodell, M., and Olivera, F.: Evaluation of the Global Land Data

644   Assimilation System using global river discharge data and a source−to−sink

645   routing scheme, Water Resour. Res., 46(6), 2010.

646   Zhang, Q., Shi, P., Singh, V.P., Fan, K., and Huang, J.: Spatial downscaling of

647   TRMM‐based precipitation data using vegetative response in Xinjiang, China,

648   Int. J. Climatol., 37(10), 3895-3909, 2017.

649   Zhou, J., Wang, L., Zhang, Y., Guo, Y., Li, X., and Liu, W.: Exploring the water

650   storage changes in the largest lake (Selin Co) over the Tibetan Plateau during

651   2003−2012 from a basin−wide hydrological modeling, Water Resour. Res.,

652   51(10), 8060-8086, 2015a.

653   Zhou, Y., Lau, W.K.M., and Huffman, G.J.: Mapping TRMM TMPA into average

654   recurrence interval for monitoring extreme precipitation events, J. Appl.

655   Meteorol. Clim., 54(5), 979-995, 2015b.

656

Table and figure captions

Table 1. The precipitation products used in this study.

Figure 1. The Upper Brahmaputra River Basin originates from the Tibetan Plateau (TP) with the spatial distribution of nine meteorological stations from the China Meteorological Administration (CMA) and 166 rain gauges from Ministry of Water Resources (MWR), China. The green arrow indicates the direction of the westerlies, the Indian monsoon and the East Asian monsoon. The elevation data was obtained from the SRTM DEM datasets (www.earthexplorer.usgs.gov).

Figure 2. The flowchart used to produce the spatio-temporal continuous precipitation dataset (*P_int*).

Figure 3. The spatial distribution of *P_int* (mm) averaged from 1981 to 2016 (a. annual; b. seasonal).

Figure 4. The spatial distribution of different precipitation products during the warm season (May to October) and the cold season (November to April) averaged from 2008 to 2016.

Figure 5. Variations in basin-averaged precipitation from multi-year monthly mean values (top), annual values (middle) and monthly values (bottom) for the different products.

Figure 6. A comparison of the probability distribution function (PDF) between all the monthly observations and different precipitation products in the warm seasons (May to October in 2014 and 2016).

Figure 7. As for Figure 6 but with scatter plots.

679 **Figure 8.** A validation of *P_int* against short time series by comparing with daily

680 gauge-averaged precipitation from May to October in 2014 and 2016.

681 **Figure 9.** A validation of *P_int* (mm) against short time series: spatial distribution of

682 the observations and corresponding grids in *P_int* from May to October in 2014 and

683 2016.

684 **Figure 10.** A validation of *P_int* against a long time series: (a). PDF and scatter plots

685 for monthly precipitation at nine CMA stations, (b). station-averaged monthly

686 precipitation from 1981 to 2016.

687 **Figure 11.** A trend analysis of the annual and seasonal precipitation (a: annual; b:

688 spring; c: summer; d: autumn; e: winter) over 36 years (1981-2016) between *P_int*,

689 GLDAS, ITP-Forcing and MERRA2. The triangles represent the observed trend of

690 the corresponding meteorological stations.

691 **Figure 12.** The number of meteorological stations (total of nine) which present the

692 same trends as the different precipitation products, according to Figure 11.

693 **Figure 13.** A comparison of extreme events, as captured by different precipitation

694 products.

695 **Figure 14.** An evaluation of simulated daily discharge at Nuxia station from 2008 to

696 2016 forced by different precipitation products. All the discharge values have been

697 normalized.

698

699   **Table 1.** The precipitation products used in this study.

Precipitation products	Time range	Temporal resolution	Spatial resolution
CMA gridded data	2008-2016	hourly	0.1°×0.1°
GLDAS	1981-2016	3-hour	0.25°×0.25°
ITP-Forcing	1981-2016	3-hour	0.1°×0.1°
MERRA2	1981-2016	hourly	0.5°×0.625°
TRMM	1998-2016	3-hour	0.25°×0.25°

700

701
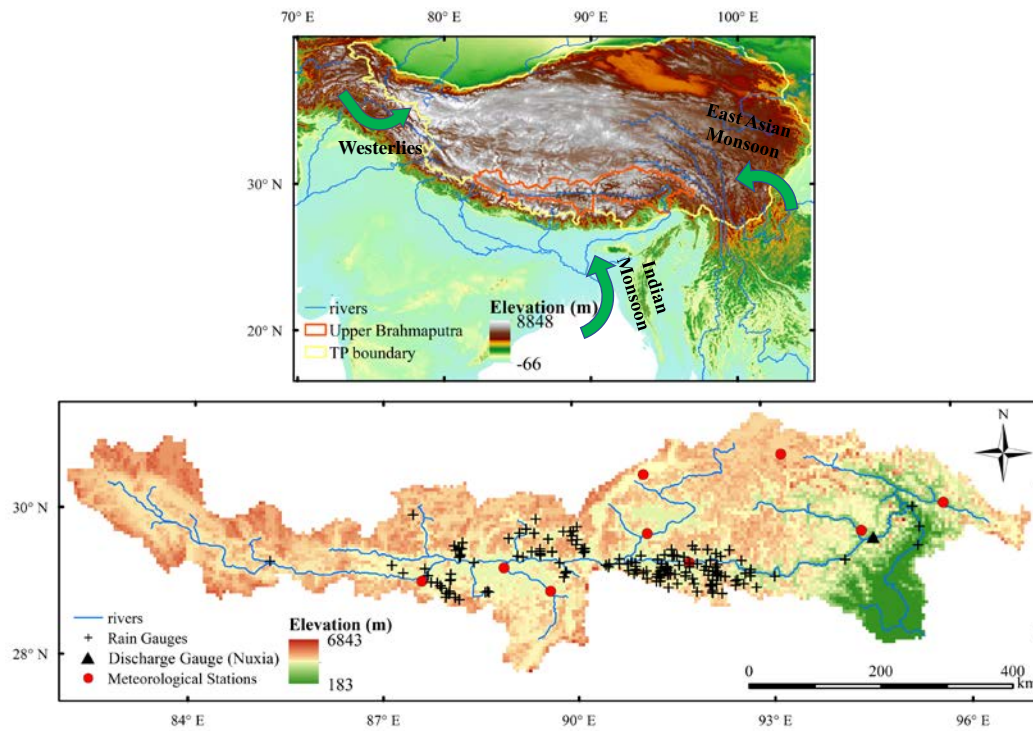
702

Figure 1. The Upper Brahmaputra River Basin originates from the Tibetan Plateau

(TP) with the spatial distribution of nine meteorological stations from the China

Meteorological Administration (CMA) and 166 rain gauges from Ministry of Water

Resources (MWR), China. The green arrow indicates the direction of the westerlies,

the Indian monsoon and the East Asian monsoon. The elevation data was obtained

from the SRTM DEM datasets (www.earthexplorer.usgs.gov).

709
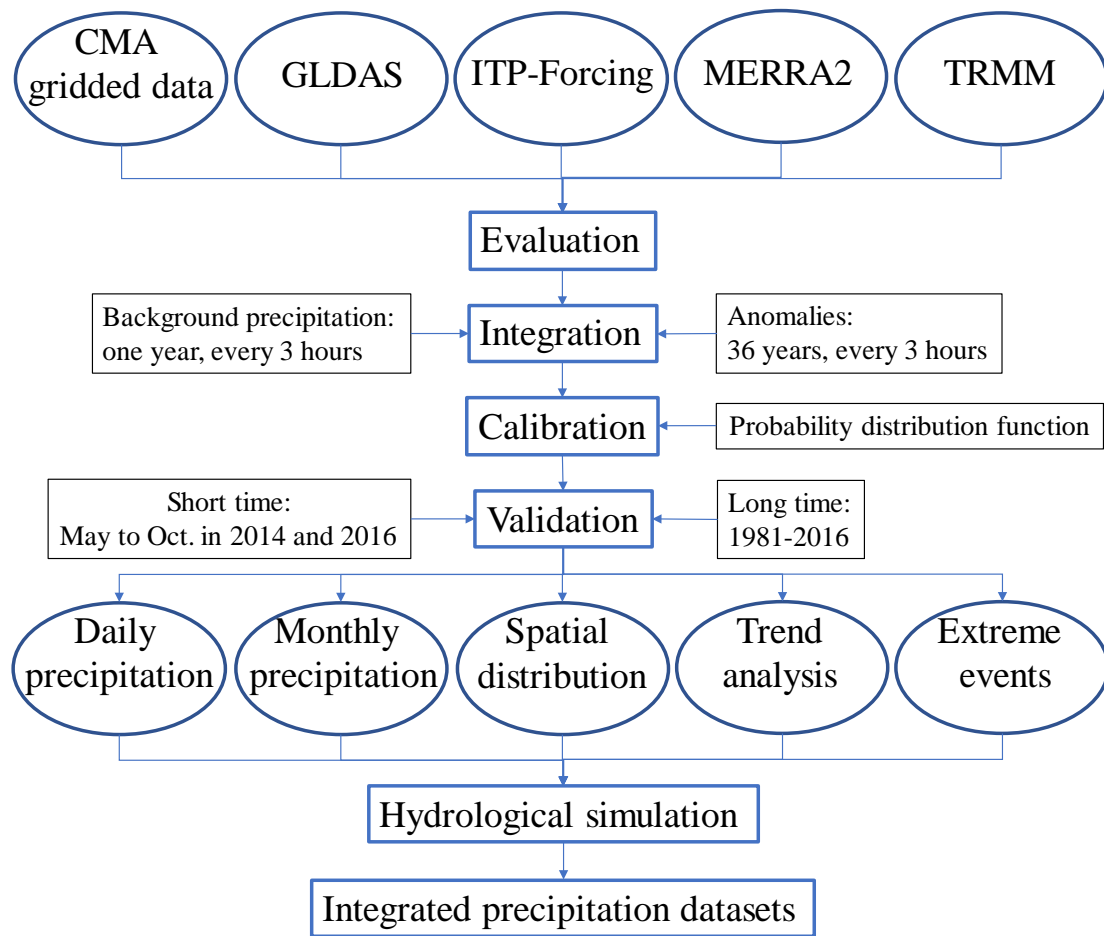
710

711 **Figure 2.** The flowchart used to produce the spatio-temporal continuous precipitation

712 dataset (*P_int*).

713
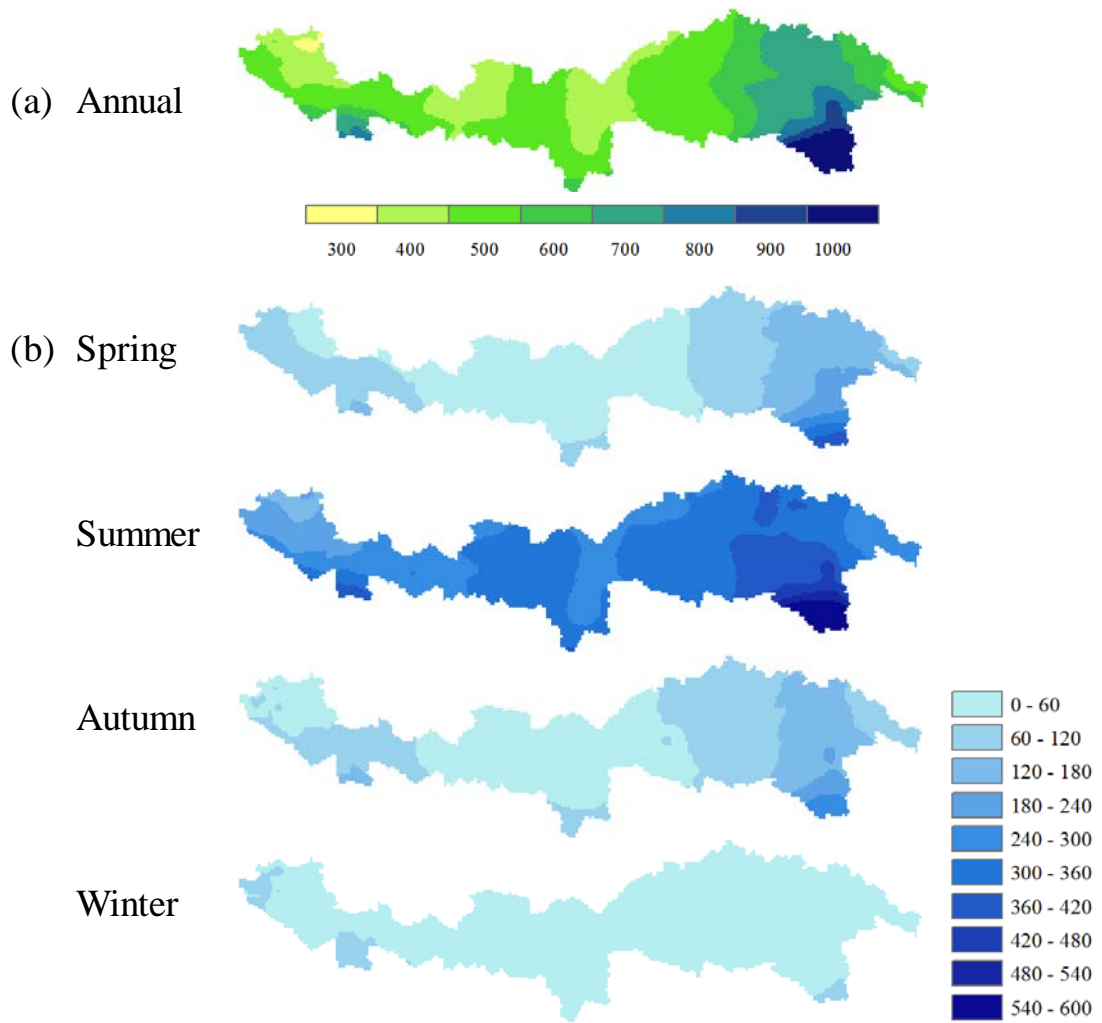
714

Figure 3. The spatial distribution of *P_int* (mm) averaged from 1981 to 2016 (a.

annual; b. seasonal).

717
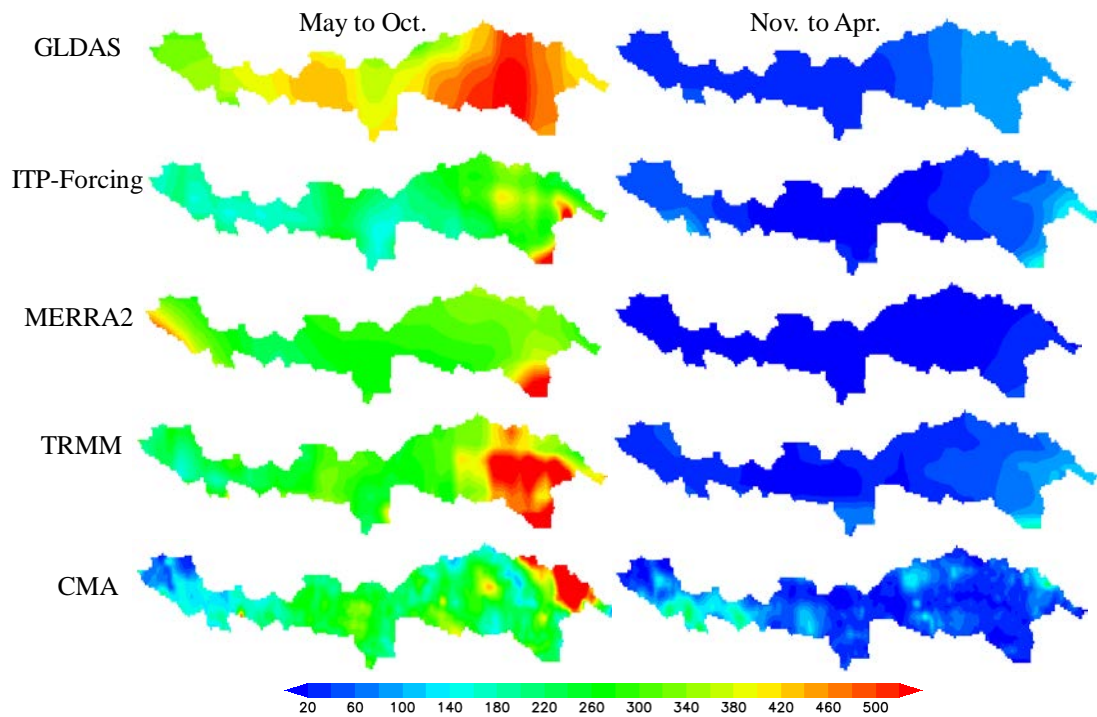
718

719 **Figure 4.** The spatial distribution of different precipitation products during the warm

720 season (May to October) and the cold season (November to April) averaged from

721 2008 to 2016.

722
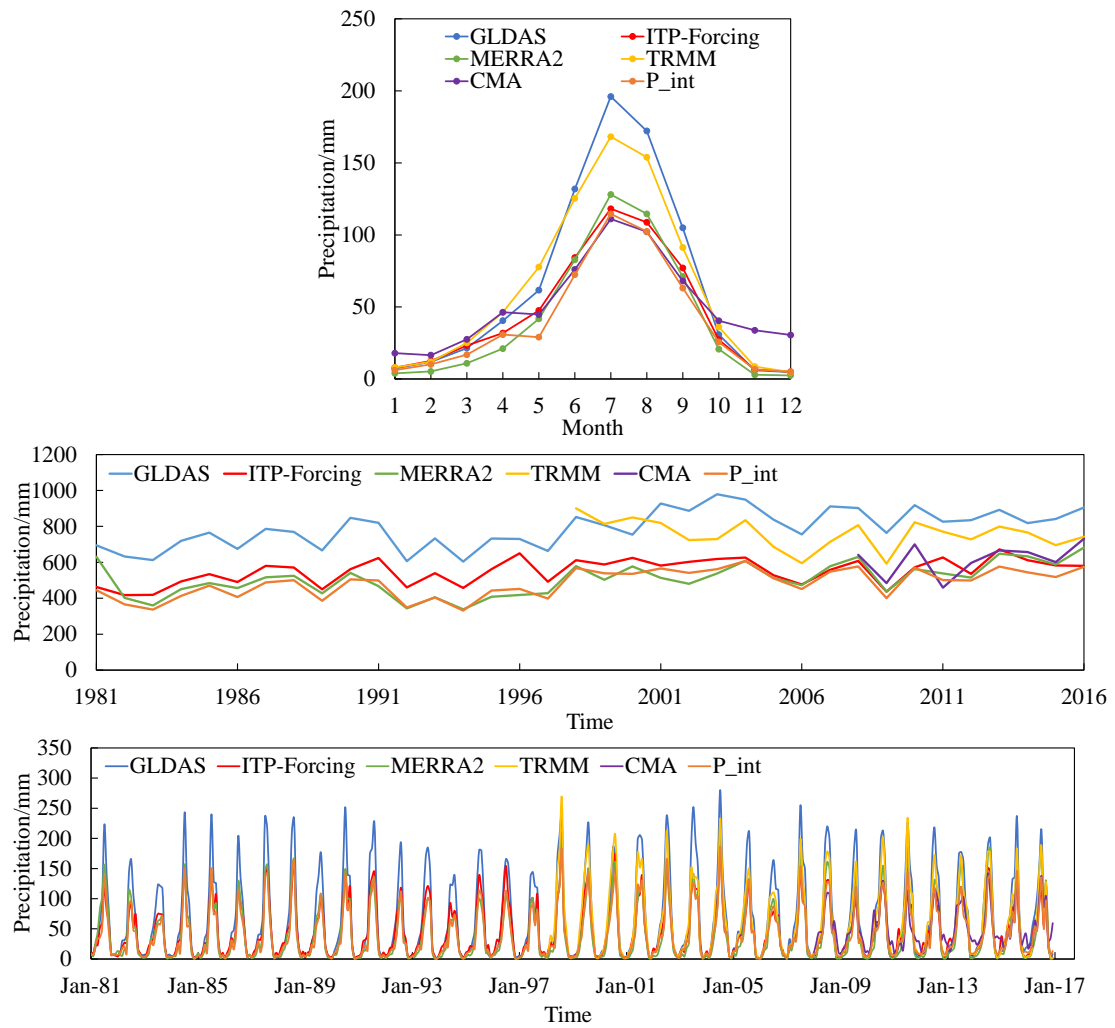
723

Figure 5. Variations in basin-averaged precipitation from multi-year monthly mean

values (top), annual values (middle) and monthly values (bottom) for the different

products.

727

728
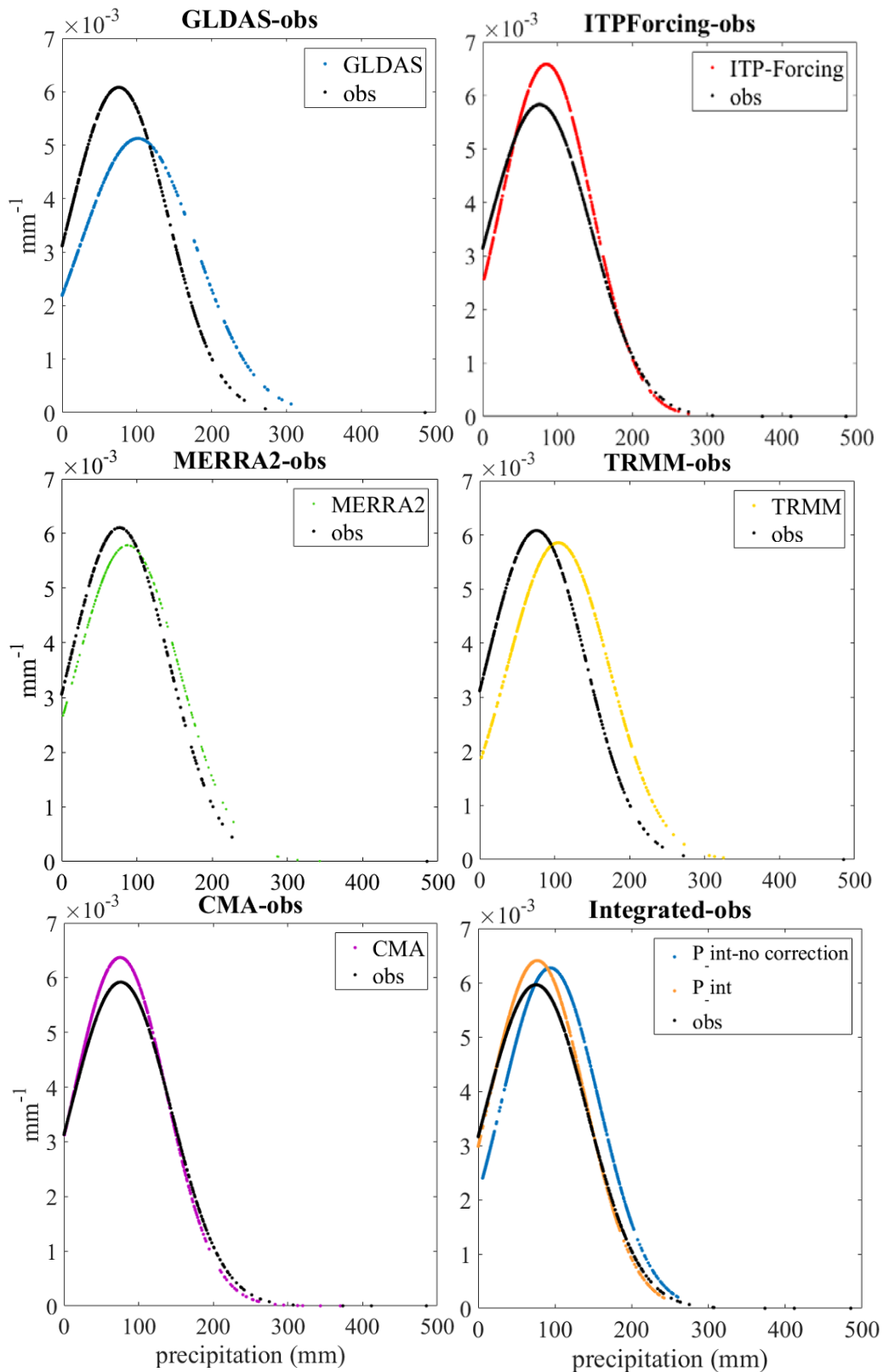
Figure 6. A comparison of the probability distribution function (PDF) between all the

monthly observations and different precipitation products in the warm seasons (May

731   to October in 2014 and 2016).

732

733
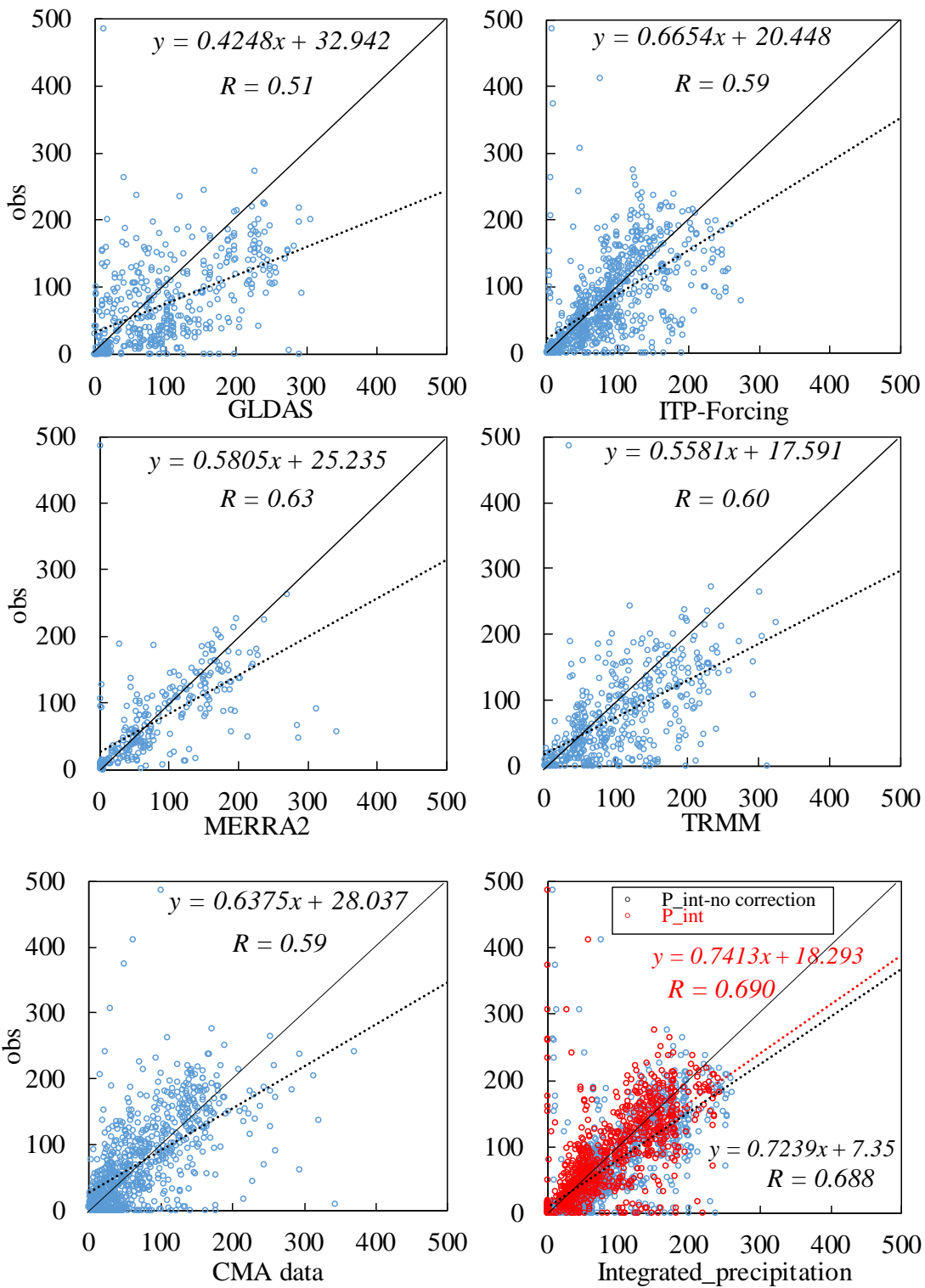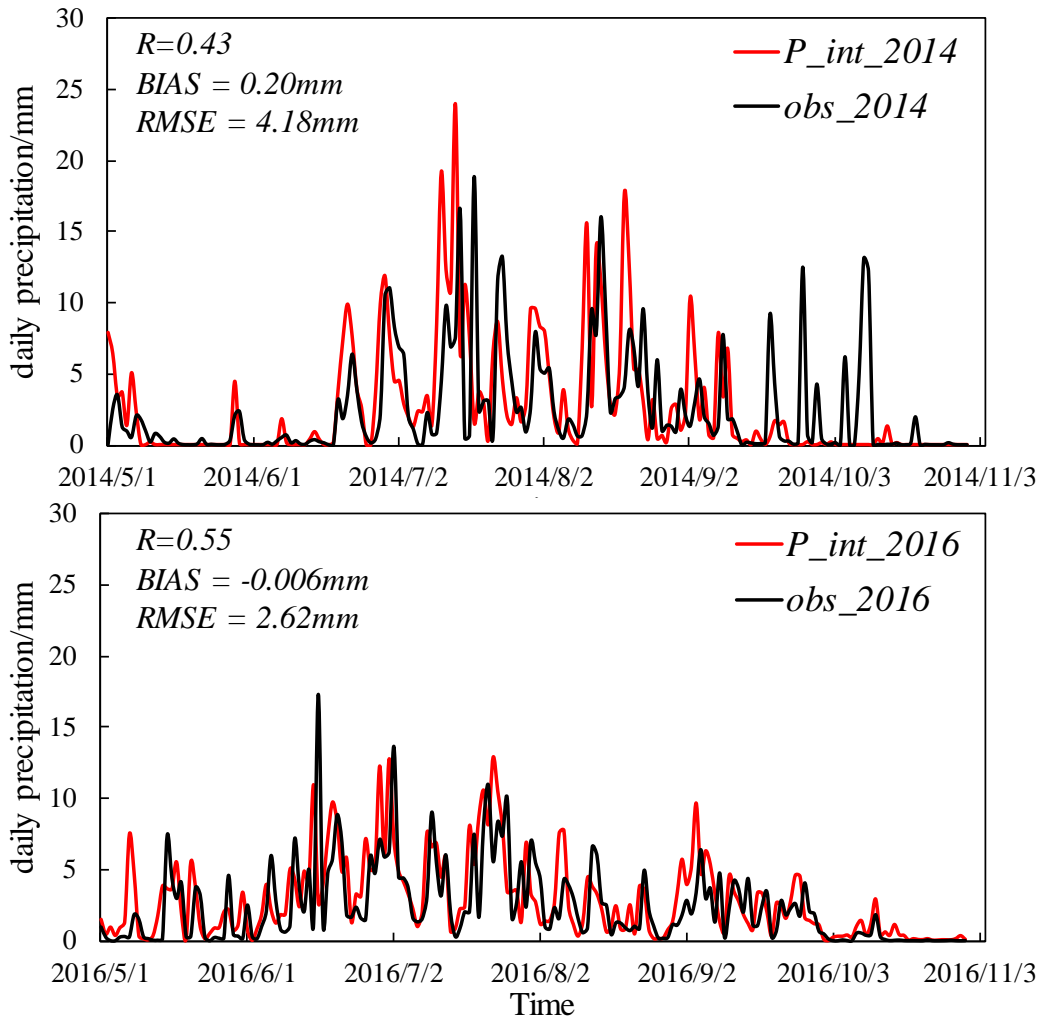
Figure 7. As for Figure 6 but with scatter plots.

735

Figure 8. A validation of *P_int* against short time series by comparing with daily

gauge-averaged precipitation from May to October in 2014 and 2016.

738
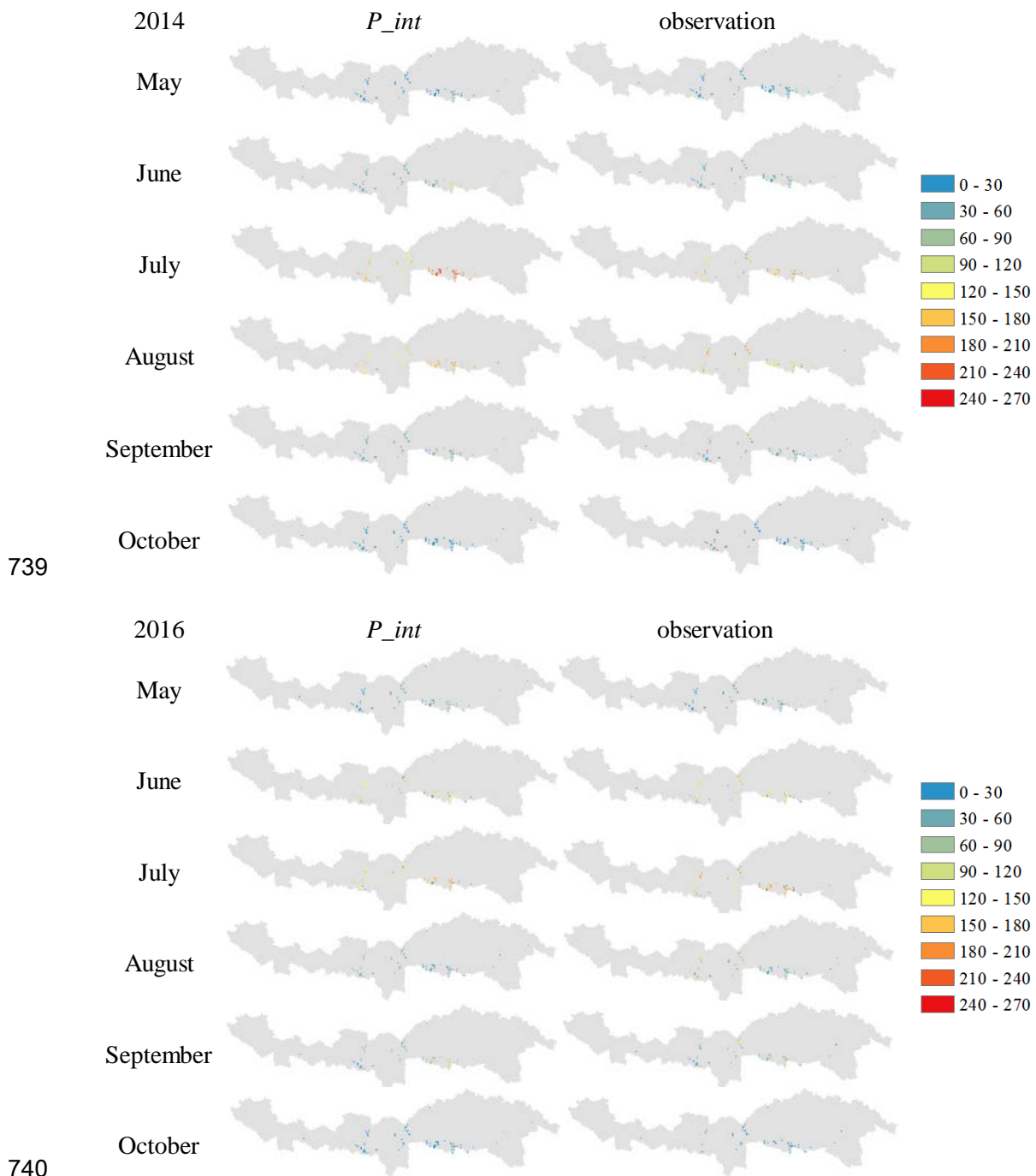
739

740

Figure 9. A validation of *P_int* (mm) against short time series: spatial distribution of

the observations and corresponding grids in *P_int* from May to October in 2014 and
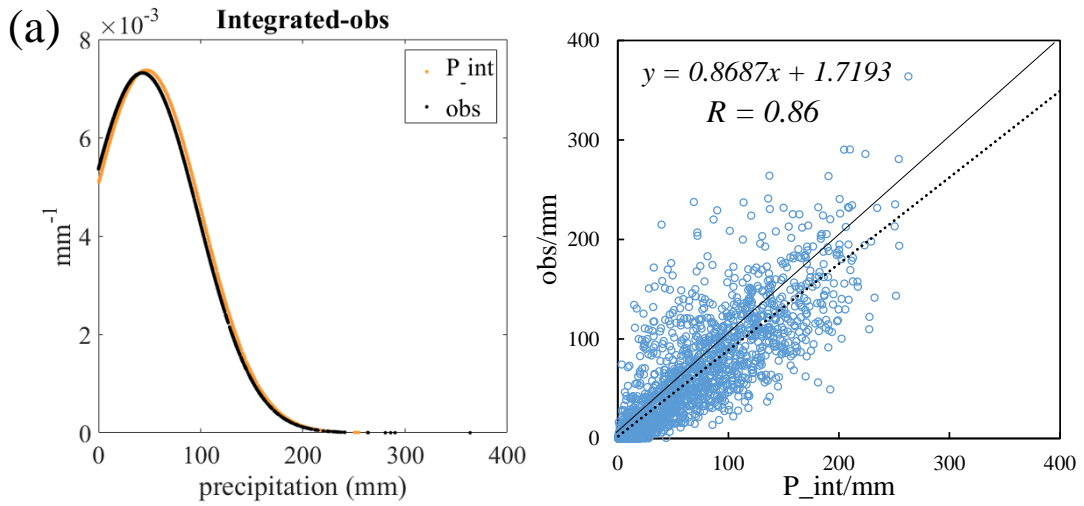
2016.

744
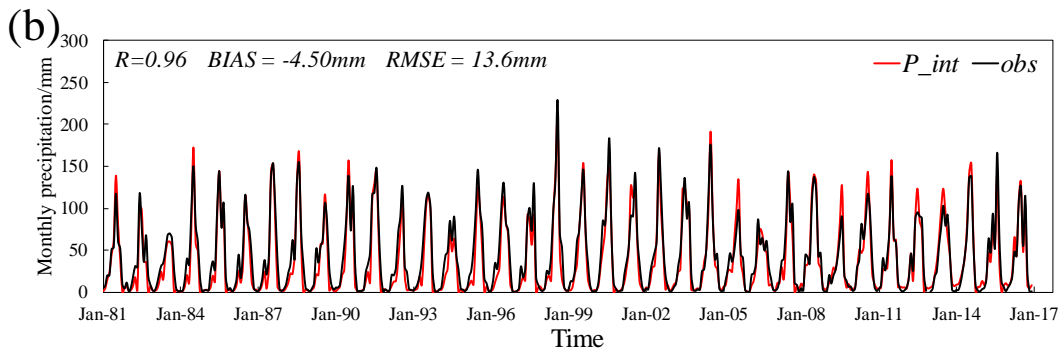
745

746 **Figure 10.** A validation of *P_int* against a long time series: (a). PDF and scatter plots

747 for monthly precipitation at nine CMA stations, (b). station-averaged monthly

748 precipitation from 1981 to 2016.

749
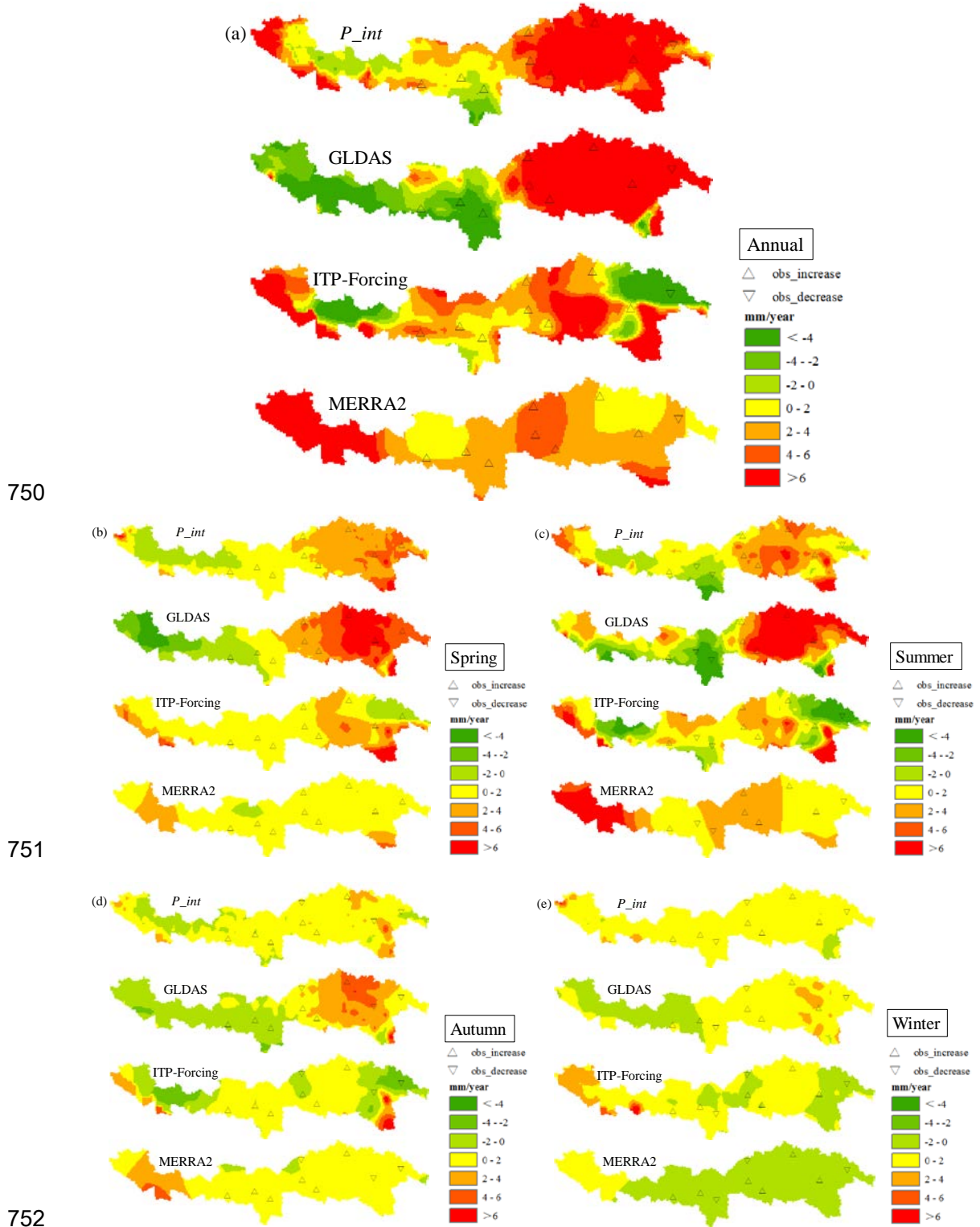
750

751

752

Figure 11. A trend analysis of the annual and seasonal precipitation (a: annual; b: spring; c: summer; d: autumn; e: winter) over 36 years (1981-2016) between *P_int*, GLDAS, ITP-Forcing and MERRA2. The triangles represent the observed trend of

756   the corresponding meteorological stations.
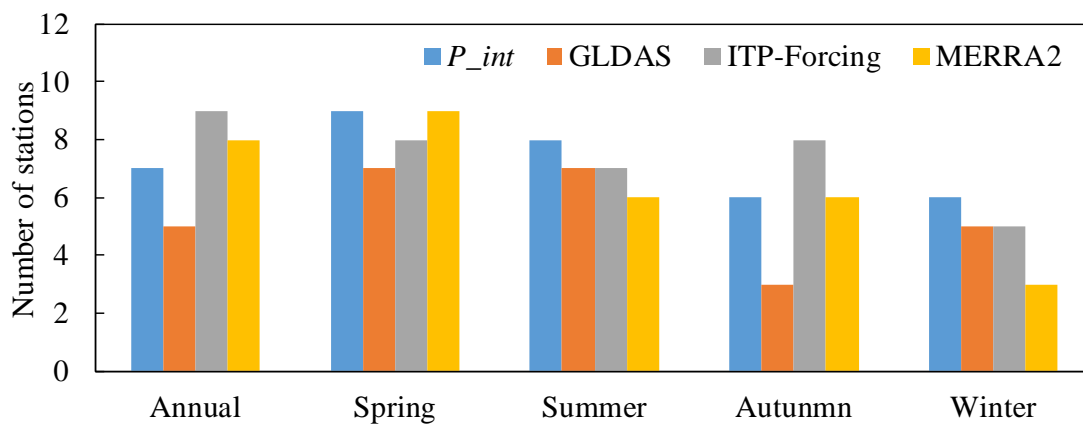
757

758   **Figure 12.** The number of meteorological stations (total of nine) which present the

759   same trends as the different precipitation products, according to Figure 11.

760
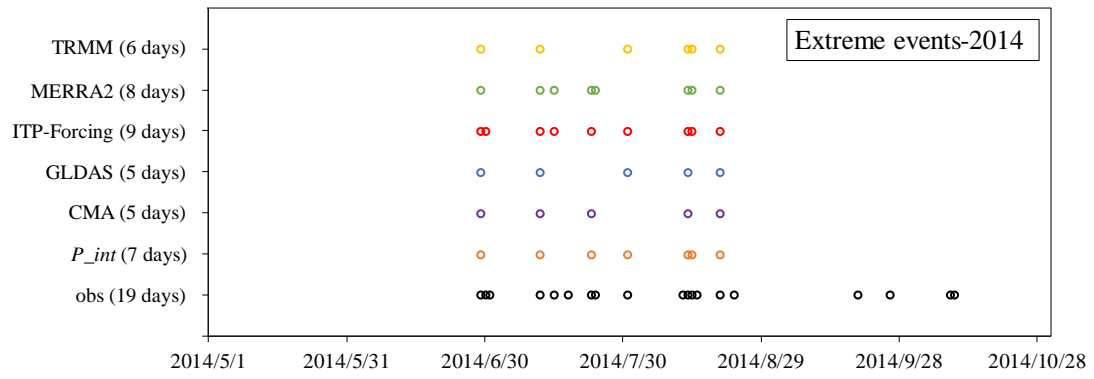
761
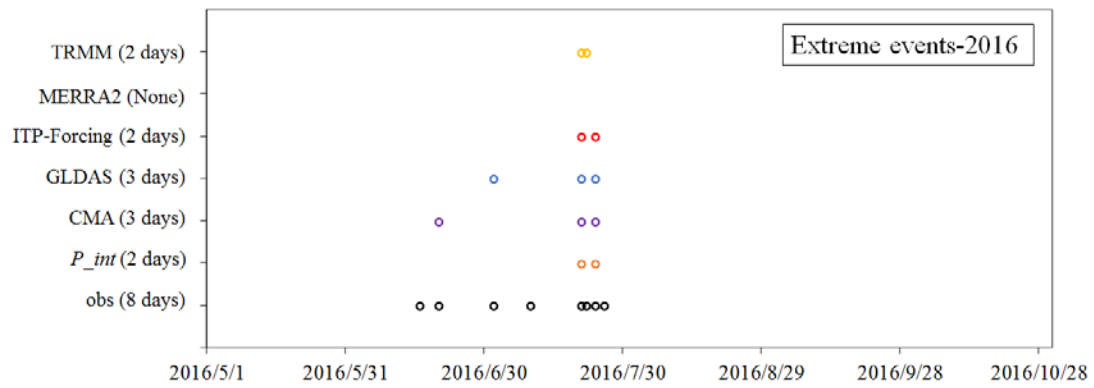
762

763 **Figure 13.** A comparison of extreme events, as captured by different precipitation

764 products.

765
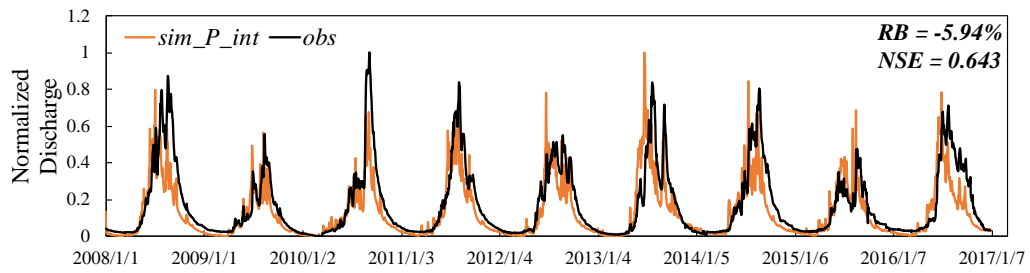
766
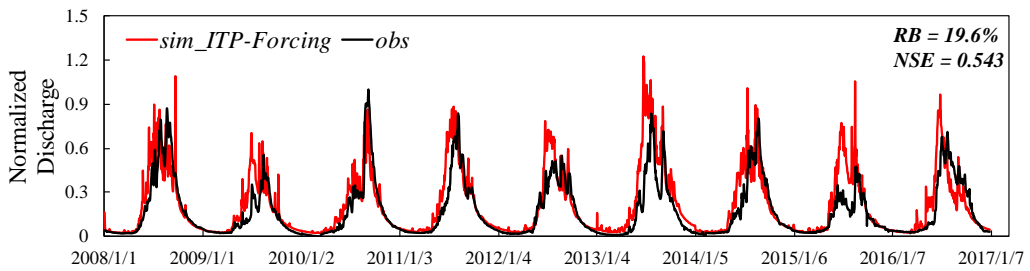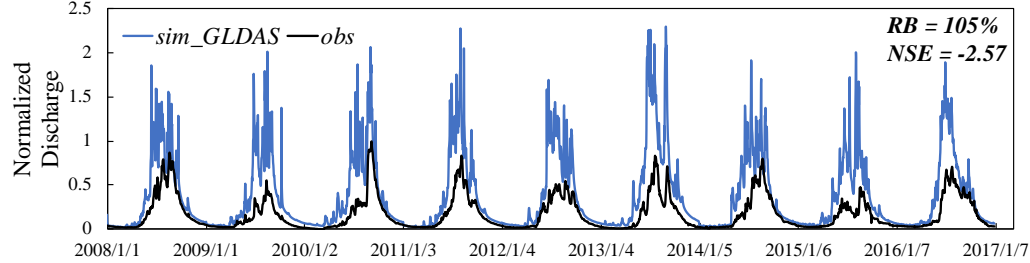
767
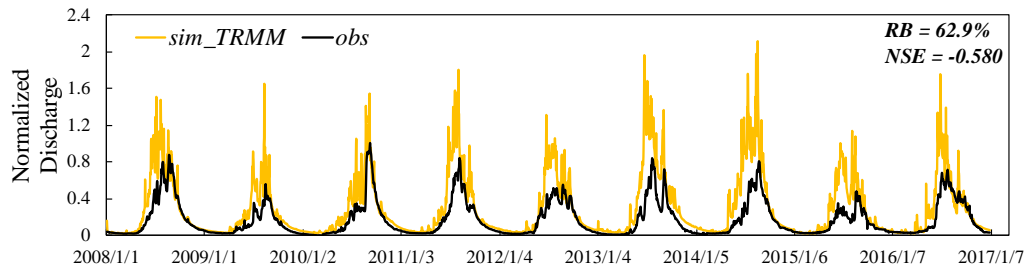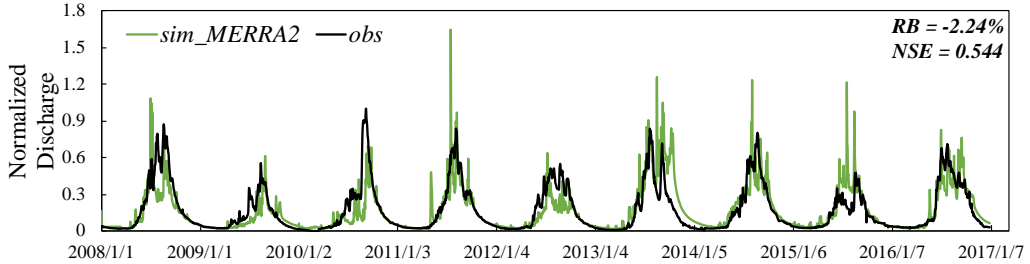
768
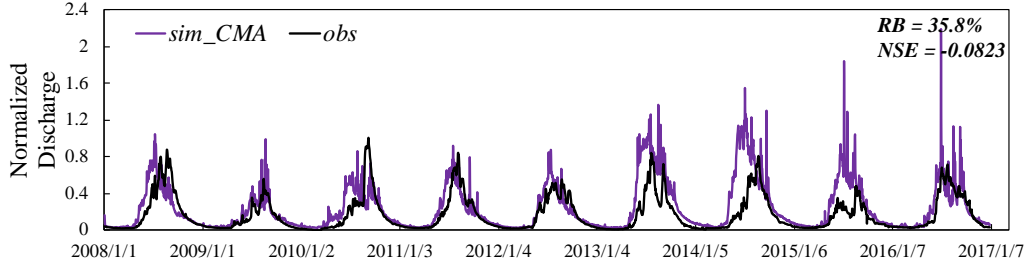
Figure 14. An evaluation of simulated daily discharge at Nuxia station from 2008 to

2016 forced by different precipitation products. All the discharge values have been

771   normalized.